Journal of Inorganic and General Chemistry
ZAAC
Zeitschrift für anorganische und allgemeine Chemie
DOI: 10.1002/zaac.202000385
ARTICLE

New Crystal Structures of Rare-Earth Metal(III) Oxotellurates(IV) $RE_2Te_3O_9$: A1-Type (RE = La, Ce) and A2-Type (RE = Pr, Nd)

Sheng-Chun Chou,[a] Patrick Höss,[a] Philip L. Russ,[a] Sabine Strobel,[a] and Thomas Schleid*[a]

Dedicated to Professor Sven Lidin on the Occasion of his 60th Birthday.

The new rare-earth metal(III) oxotellurates(IV) $RE_2Te_3O_9$ (RE = La–Nd) of the so far unknown A-type structure can be obtained as needle-shaped single crystals through solid-state reactions of the corresponding binary oxides. Their crystal structures were determined as A1-type for RE = La and Ce or A2-type for RE = Pr and Nd by single-crystal X-ray diffraction. Both structure types crystallize in the monoclinic crystal system, but in two different non-centrosymmetric space groups: the A1-type with Z = 8 in space group $P2_1$ ($La_2Te_3O_9$: a = 569.54(3), b = 2230.12(13), c = 1464.71(4) pm, β = 101.205(3)°; $Ce_2Te_3O_9$: a = 567.02(3), b = 2222.61(13), c = 1457.13(9) pm, β = 101.134(3)°) or the A2-type with Z = 16 in space group Cc ($Pr_2Te_3O_9$: a = 2838.61(16), b = 563.89(3), c = 2522.08(15) pm, β = 118.816(3)°; $Nd_2Te_3O_9$: a = 2826.38(16), b = 561.47(3), c = 2511.94(15) pm, β = 118.841(3)°). In spite of the differences in the unit-cell parameters and the symmetry, both structures consist of quite similar fundamental building blocks (FBBs) consisting of eight crystallographically distinct rare-earth metal-oxygen polyhedra with C.N.(RE^{3+}) from seven to nine and always twelve different ψ^1-tetrahedral oxotellurate(IV) anions $[TeO_3]^{2-}$, which show a high number of secondary bonding interactions (SBIs) with each other in all four cases.

Introduction

Tellurium(IV) oxides and oxotellurates(IV) are attracting more and more research attention, because they can adopt unusual crystal structures. Some examples are $NdClTe_2O_5$ (tetragonal, $P4/mmm$)[1] with ψ^1-octahedrally coordinated Te^{4+} cations, α-TeO_2 (paratellurite: tetragonal, $P4_12_12$)[2] and β-TeO_2 (tellurite: orthorhombic, $Pbca$)[3] and high-pressure γ-TeO_2 (orthorhombic, $P2_12_12_1$)[4] with ψ^1-trigonal bipyramidally coordinated Te^{4+} cations, $Zn[TeO_3]$ (orthorhombic, $Pbca$)[5] with discrete ψ^1-tetrahedral $[TeO_3]^{2-}$ anions and $Ca(Mn,Zn)[Te_2O_5]_2$ (as mineral denningite: tetragonal, $P4_2/nbc$)[6] with pyroanionic $[Te_2O_5]^{2-}$ groups. This is mainly due to the variability in the coordination environments of the oxotellurate(IV) anion[7–9] and also the presence of a stereochemically active lone-pair of electrons at their Te^{4+} centers. These lone pairs can serve as an invisible structure-directing ligands,[10–12] which often lead to non-centrosymmetric structures (NCS) with interesting physical properties, such as non-linear optical second harmonic generation (SHG), piezo-, pyro- and ferroelectricity.[13–17] When compared to the related oxosulfates(IV), oxoarsenates(III) and oxoselenates(IV) with third and fourth period members of the periodic system of the elements (PSE), which also contain lone-pair electrons in their ψ^1-tetrahedral $[SO_3]^{2-}$, $[AsO_3]^{3-}$ and $[SeO_3]^{2-}$ anions, oxotellurates(IV) groups exhibit strong $Te^{4+}\cdots O^{2-}$ secondary bonding interactions (SBIs) between the analogous $[TeO_3]^{2-}$ anions and thus show much better thermal and chemical stabilities. Therefore, they are also promising host-lattice choices for phosphor materials used in monochromatic or white light LED applications in light-emitting diodes.[18]

Recently we have prepared and characterized several ternary rare-earth metal(III) oxotellurates(IV) in our group already. They are known with different compositions depending on the molar ratio RE_2O_3:TeO_2, and their general formula can thus be described as $RE_2O_3(TeO_2)_n$. Up to now many tellurium-dioxide rich compounds, namely $RE_2Te_4O_{11}$ (n = 4; RE = Sc, Y, La–Lu)[19–27] and $RE_2Te_5O_{13}$ (n = 5; RE = Sc, Y, Dy–Lu),[26–30] have been structurally characterized. In contrast, for the composition $RE_2Te_3O_9$ (n = 3) rather few representatives are known so far and with n = 2, only $Pr_2Te_2O_7$ was reported, which contains oxygen atoms not bonded to any Te^{4+} cation according to $Pr_2O[TeO_3]_2$.[31] It was first suggested by *Redman et al.* that three different structure types should exist for the composition $RE_2Te_3O_9$, depending on the size of the involved RE^{3+} cation: the A-type for RE = La–Nd, the B-type for RE = Y, Sm–Er and the C-type for RE = Tm–Lu.[32] The B-type crystallizes in the monoclinic space group $P2_1/c$, which has four crystallographically independent RE^{3+} cations surrounded by seven and eight oxygen atoms.[33–36] In contrast, the C-type crystallizes in the triclinic space group $P\bar{1}$ with six different RE^{3+} positions, which are again surrounded by seven and eight oxygen atoms.[33–35,37,38] Finally, the D-type crystallizes in the monoclinic space group $P2_1/n$ with two crystallographically distinct RE^{3+}

[a] S.-C. Chou, P. Höss, P. L. Russ, S. Strobel, Prof. Dr. Th. Schleid
Institut für Anorganische Chemie, Universität Stuttgart
Pfaffenwaldring 55, D-70569 Stuttgart, GermanyFax: +49(0)711/685-64241
E-mail: schleid@iac.uni-stuttgart.de

cations coordinated by six and seven oxygen atoms, which restricts it to *RE* = Sc[34,39,40] so far. It was assumed that $La_2Te_3O_9$ and $Ce_2Te_3O_9$ comprise the same A-type crystal structure as their analogue $Nd_2Te_3O_9$ (monoclinic, space group: *Cc*).[33] Now were able to synthesize single crystals of $La_2Te_3O_9$ and $Ce_2Te_3O_9$ for the first time. The single crystal-structure determination and refinement proves that they have a new crystal structure, while $Pr_2Te_3O_9$ was also synthesized and determined to crystallize in the same structure as $Nd_2Te_3O_9$. Due to the fact that both the structures of $La_2Te_3O_9$ and $Ce_2Te_3O_9$ as well as those of $Pr_2Te_3O_9$ and $Nd_2Te_3O_9$ have a lot in common (Figure 1), the denomination A1-type and A2-type structure, respectively, was chosen for nomenclature and differentiation. In this article we present the synthesis and crystal structure of the A1-type (*RE* = La, Ce) and the A2-type (*RE* = Pr, Nd) arrangements for the composition $RE_2Te_3O_9$ and a discussion of their structural similarities and differences.

Results and Discussion

Structure Description of A1-Type $RE_2Te_3O_9$ (RE = La and Ce)

Both $La_2Te_3O_9$ and $Ce_2Te_3O_9$ crystallize monoclinically in the non-centrosymmetric space group $P2_1$ ($La_2Te_3O_9$: $a = 569.54(3)$, $b = 2230.12(13)$, $c = 1464.71(4)$ pm, $\beta = 101.205(3)°$; $Ce_2Te_3O_9$: $a = 567.02(3)$, $b = 2222.61(13)$, $c = 1457.13(9)$ pm, $\beta = 101.134(3)°$) with eight formula units per unit cell. They represent the new A1-type crystal structure for the composition $RE_2Te_3O_9$ with all atoms residing at the general *Wyckoff* position 2*a* (site symmetry: 1). The eight crystallographically distinguishable RE^{3+} cations are seven-, eight- and ninefold coordinated by oxygen atoms with RE^{3+}–O^{2-} distances ranging from 240 to 302 pm for *RE* = La (Tables 7–10) and from 234 to 302 pm for *RE* = Ce, which are in good accordance with $La_2Te_4O_{11}$ ($d(La^{3+}$–$O^{2-}) = 242$–267 pm) and $Ce_2Te_4O_{11}$ ($d(Ce^{3+}$–$O^{2-}) = 239$–265 pm),[22] respectively. The coordination polyhedra of the *RE*1 and *RE*2 cations can be described as bicapped trigonal prisms with a ninth oxygen atom at a rather long distance (d(*RE*1–O17) = 290 pm (*RE* = La), 291 pm (*RE* = Ce); d(*RE*2–O21) = 302 pm (*RE* = La), 302 pm (*RE* = Ce)), which results in C.N. = 8 + 1. The cations *RE*3–*RE*7 are coordinated with eight oxygen atoms each in the shape of trigonal dodecahedra (*RE*3), square antiprisms (*RE*4 and *RE*5) or bicapped trigonal prism (*RE*6 and *RE*7). Just the cation *RE*8 exhibits only a sevenfold coordination of oxygen atoms forming a monocapped trigonal prism (Figure 2). All lanthanide-oxygen polyhedra are condensed as fundamental building blocks (FBBs) to layers following a rather complicated linking pattern. Their basic elements can be best described via five types of zigzag chains running along the [100] direction, which are each built of two kinds of alternating polyhedra by sharing common vertices and edges. The first chain consists of $[(RE1)O_8]^{13-}$ and $[(RE4)O_8]^{13-}$, which are connected via vertices and edges formed by O36 and O11···O18, the second one of $[(RE1)O_8]^{13-}$ and $[(RE7)O_8]^{13-}$ linked via O32 and O1···O19, the third one of $[(RE2)O_8]^{13-}$ and $[(RE5)$-

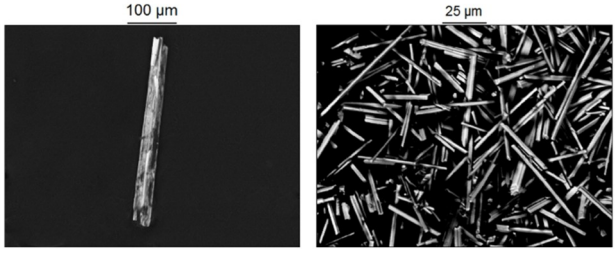

Figure 1. Scanning electron microscope (SEM) images of A1-type $La_2Te_3O_9$ (*left*) and A2-type $Nd_2Te_3O_9$ (*right*) as needle-shaped crystals with high aspect ratio. All compounds of the short $RE_2Te_3O_9$ series (*RE* = La–Nd) have this habit in common, owing to their short *a*- or *b*-axes, along which the crystals grow fastest.

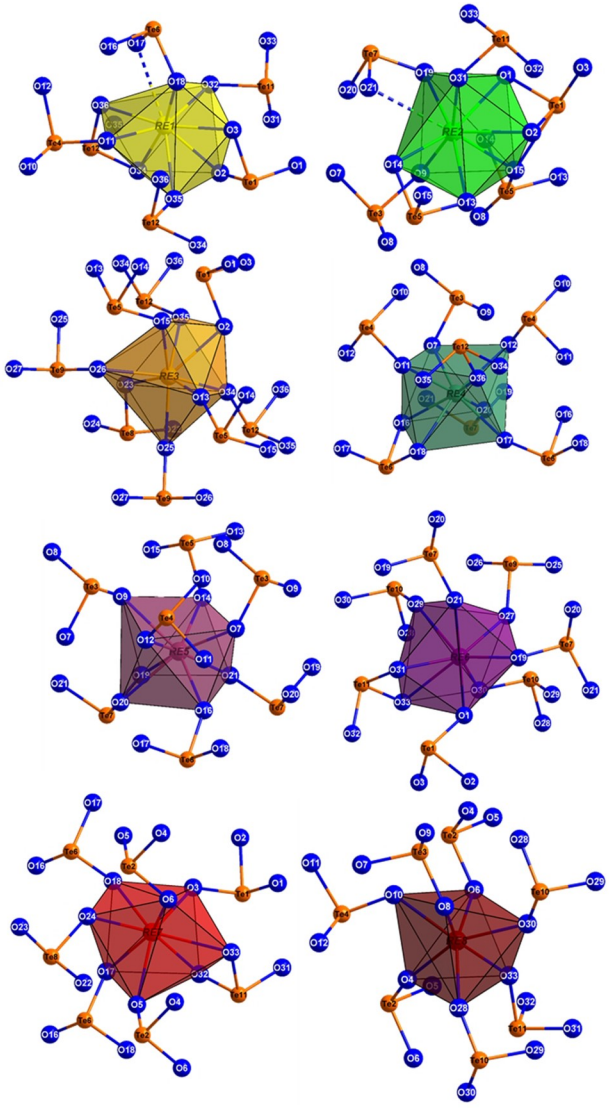

Figure 2. Oxygen coordination polyhedra of the eight crystallographically independent RE^{3+} cations (*RE* = La and Ce) in the A1-type crystal structure for the composition $RE_2Te_3O_9$ along with the attached ψ^1-tetrahedral $[TeO_3]^{2-}$ anions.

$O_8]^{13-}$ connected by O14 and O9···O19, the fourth one contains $[(RE2)O_8]^{13-}$ and $[(RE6)O_8]^{13-}$ with shared O31 and O1···O19 linkers, thereby they forming $^1_\infty\{[RE_2O_{13}]^{20-}\}$ chains. The last one, consisting of $[(RE4)O_8]^{13-}$ and $[(RE5)O_8]^{13-}$ fused by O7···O16 and O12···O20 edges, represents a $^1_\infty\{[RE_2O_{12}]^{18-}\}$ chain. The chains with *RE*1–*RE*4 and *RE*1–*RE*7 form the first double chain by sharing edges O17···O18 (between $[(RE4)O_8]^{13-}$ and $[(RE7)O_8]^{13-}$), while those containing *RE*2–*RE*5- and *RE*2–*RE*6 are condensed to the second double chain via common edges O19···O21 (between $[(RE5)O_8]^{13-}$ and $[(RE6)O_8]^{13-}$), both with channels along the [100] direction. These two kinds of double chains are further linked through common vertices O2 (between $[(RE1)O_8]^{13-}$ and $[(RE2)O_8]^{13-}$) and O33 (between $[(RE6)O_8]^{13-}$ and $[(RE7)O_8]^{13-}$) thus generating the basic layers of the A1-type crystal structure. The last two types of polyhedra $[(RE3)O_8]^{13-}$ and $[(RE8)O_7]^{11-}$ are then attached to these basic layers from above and below in the channels of the double chains by sharing common edges O2···O35 (for $[(RE1)O_8]^{13-}$ and $[(RE3)O_8]^{13-}$), O2···O15 (for $[(RE2)O_8]^{13-}$ and $[(RE3)O_8]^{13-}$), O30···O33 (for $[(RE6)O_8]^{13-}$ and $[(RE8)O_7]^{11-}$) and O6···O33 (for $[(RE7)O_8]^{13-}$ and $[(RE8)O_7]^{11-}$), respectively. Finally, thick serrated $^2_\infty\{[RE_8O_{35}]^{46-}\}$ profile layers parallel to the (010) plane emerge in the crystal structure of A1-type $RE_2Te_3O_9$ (*RE* = La and Ce; Figure 3, *left*). Each $^2_\infty\{[RE_8O_{35}]^{46-}\}$ sheet is related to its neighboring layers of the same kind by a 2_1 screw axis and stacked along the crystallographic *b*-axis following a lock-and-key model (Figure 3, *top right*).

The oxotellurate(IV) partial structure of A1-type $RE_2Te_3O_9$ with *RE* = La and Ce contains twelve crystallographically independent Te^{4+} cations. Each one is bonded to three oxygen atoms (d(Te–O) = 179–196 pm) in its primary coordination sphere. Together with the stereochemically active lone-pair of electrons they form the typical ψ^1-tetrahedrally shaped $[TeO_3]^{2-}$ anions involving all the 36 independent oxygen atoms. Furthermore, strong secondary Te^{4+}···O^{2-} interactions (d(Te···O) = 250–297 pm), which are generally common for all rare-earth metal(III) oxotellurates(IV), are also present in the A1-type crystal structure for the $RE_2Te_3O_9$ members. Thus, the coordination numbers of Te1–Te4 rise to C.N. = 3 + 2, whereas Te5–Te11 have one secondary contact to their adjacent oxotellurate(IV) units resulting in C.N. = 3 + 1. In $La_2Te_3O_9$ and $Ce_2Te_3O_9$ for Te12 no secondary bonding interactions (SBIs) can be observed, however (Figure 4). Nevertheless, through these secondary Te^{4+}···O^{2-} contacts, eleven of the $[TeO_3]^{2-}$ anions are bound together to form $^1_\infty\{[Te_{11}O_{33}]^{22-}\}$ strands along the crystallographic [100] direction leaving only the last oxotellurate(IV) anion $[(Te12)O_3]^{2-}$ isolated behind. Although in $La_2Te_3O_9$ and $Ce_2Te_3O_9$ Te12 has no SBI to its adjacent oxotellurate(IV) units, the $[(Te12)O_3]^{2-}$ groups are donatively attached to this strand through the secondary coordination sphere of Te1 (d(Te1···O34), respectively. The $^1_\infty\{[Te_{11}O_{33}]^{22-}\}$ strands decorated with $[(Te12)O_3]^{2-}$ units, which are stacked along the [010] direction (Figure 5) in the same way like their rare-earth metal-oxygen counterparts, make up the oxotellurate(IV) partial structure of A1-type $La_2Te_3O_9$ and $Ce_2Te_3O_9$ with one-dimensional character. In addition, O–Te–O angles from 88 to 104° (Tables 11–14) deflect the Te^{4+} cations out of their triangular (O,O,O)-plane by values from 86 to 107 pm.

The displacement parameters are listed for the A1-type in Tables 3–6.

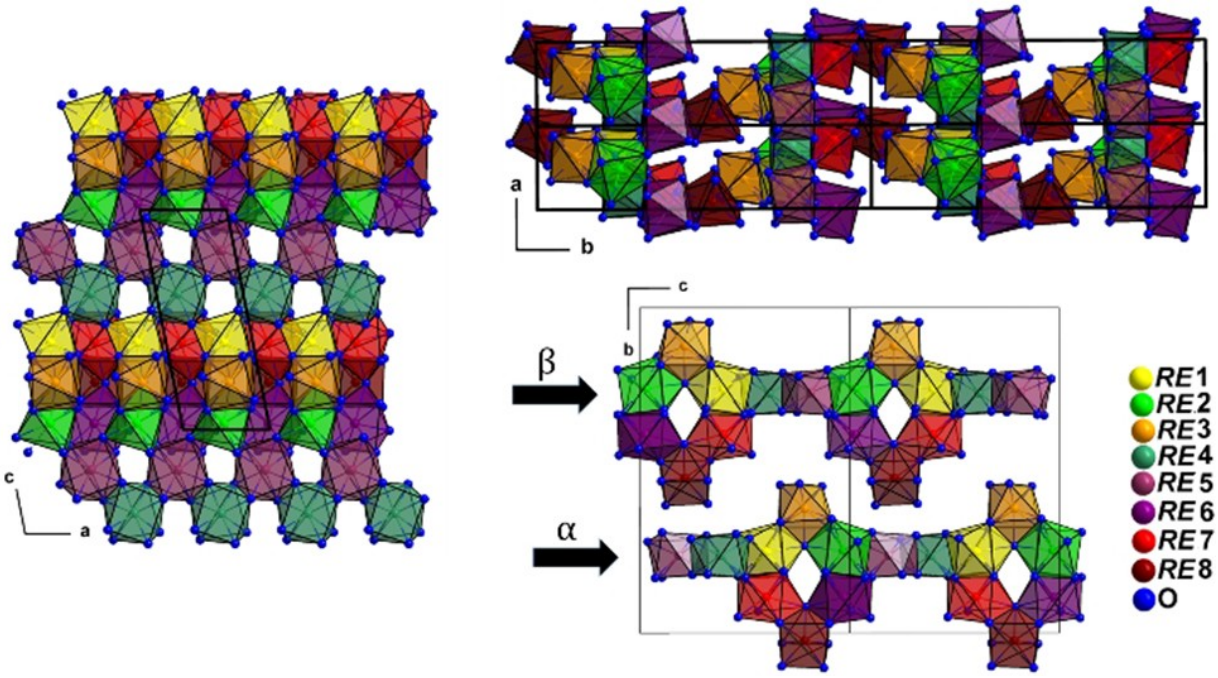

Figure 3. Five chains ($4\times^1_\infty\{[RE_2O_{13}]^{20-}\}$ and $1\times^1_\infty\{[RE_2O_{12}]^{18-}\}$) forming corrugated $^2_\infty\{[RE_8O_{35}]^{46-}\}$ layers parallel to the (010) plane in the A1-type crystal structure (*left*) for the composition $RE_2Te_3O_9$ (*RE* = La and Ce). The graph shows these serrated $^2_\infty\{[RE_8O_{35}]^{46-}\}$ sheets in top view of α- and β-layers parallel to the (100) plane (*bottom right*) and the side view of the twofold axis parallel to the (001) plane (*top right*).

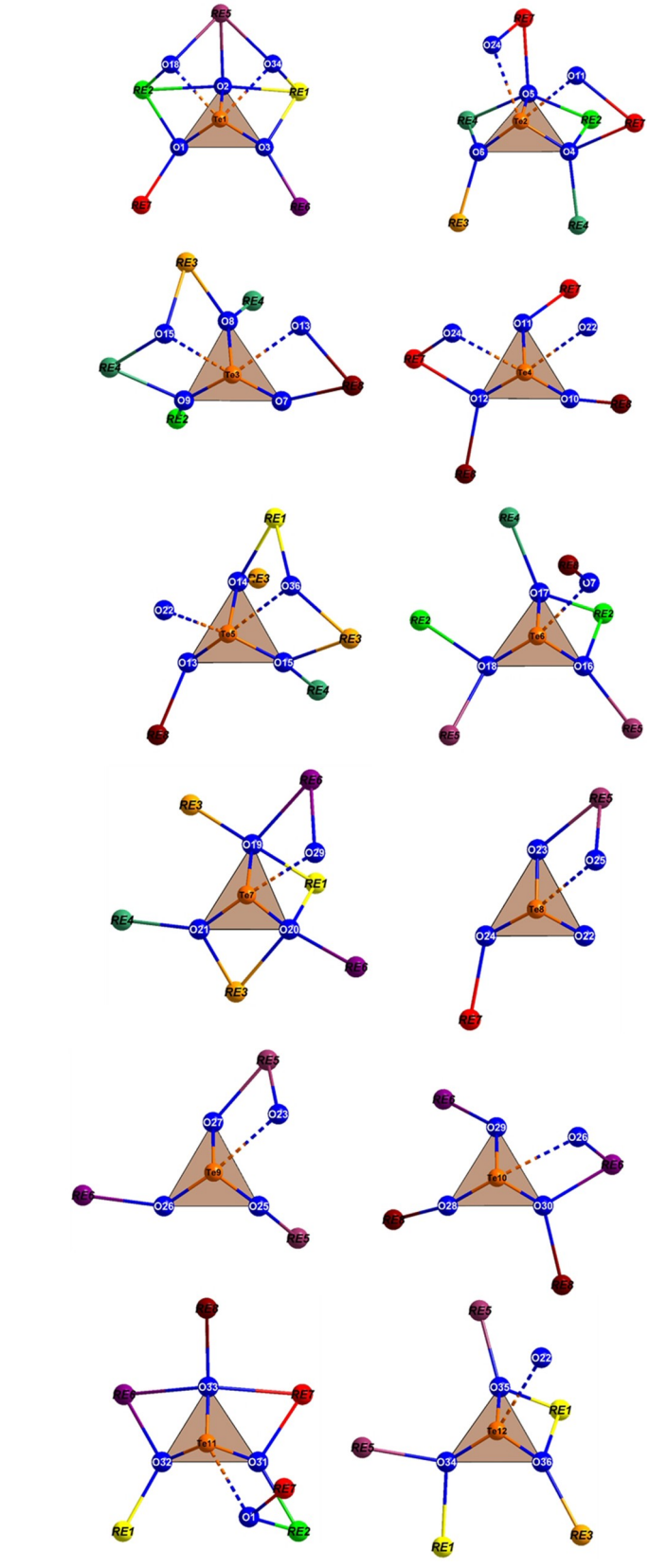

Figure 4. Coordination polyhedra of the twelve crystallographically different Te^{4+} cations in the A1-type crystal structure for the composition $RE_2Te_3O_9$ (*RE* = La and Ce), where eleven $[TeO_3]^{2-}$ units are linked through strong secondary $Te^{4+}\cdots O^{2-}$ contacts (*dashed bonds*), with their complete cationic surrounding.

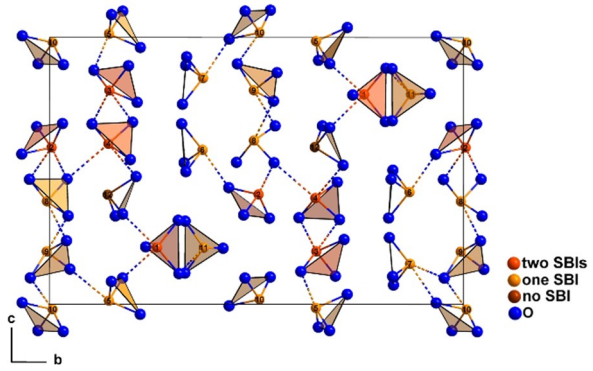

Figure 5. Through several strong secondary $Te^{4+}\cdots O^{2-}$ contacts $^1_\infty\{[Te_{11}O_{33}]^{22-}\}$ strands are formed in the A1-type crystal structure for the composition $RE_2Te_3O_9$ (*RE* = La and Ce) propagating along the [100] direction and leaving only the $[(Te12)O_3]^{2-}$ anions isolated behind.

Structure Description of A2-Type $RE_2Te_3O_9$ (RE = Pr and Nd)

$Pr_2Te_3O_9$ crystallizes isostructurally to $Nd_2Te_3O_9$[33] in the monoclinic non-centrosymmetric space group *Cc* ($Pr_2Te_3O_9$: a = 2838.61(16), b = 563.89(3), c = 2522.08(15) pm, β = 118.816(3)°; $Nd_2Te_3O_9$: a = 2826.38(16), b = 561.47(3), c = 2511.94(15) pm, β = 118.841(3)°) with sixteen formula units per unit cell. Their crystal structures were assigned as A2-type for the composition $RE_2Te_3O_9$ with all atoms located at the general *Wyckoff* position 4*a* (site symmetry: 1). Just like for the A1-type cases they contain eight crystallographically different RE^{3+} cations in nine- (*RE*1 and *RE*2: bicapped trigonal prisms plus one more distant oxygen atom), eight- (*RE*3 and *RE*4: square antiprisms, *RE*5: bicapped trigonal prism, *RE*6: trigonal dodecahedron; *RE*7: bicapped trigonal prism), and sevenfold (*RE*8: monocapped trigonal prism) oxygen coordination (Figure 6). Their interatomic distances between RE^{3+} and O^{2-} (d = 236–289 pm for *RE* = Pr, d = 233–285 pm for *RE* = Nd) correlate well with those in $Pr_2Te_4O_{11}$ ($d(Pr^{3+}\text{–}O^{2-})$ = 238–262 pm) and $Nd_2Te_4O_{11}$ ($d(Nd^{3+}\text{–}O^{2-})$ = 237–261 pm),[22] respectively (Tables 7–10). All lanthanide-oxygen polyhedra, which look almost identical in shape to those in the A1-type $RE_2Te_3O_9$ cases with *RE* = La and Ce, are interconnected to form $^2_\infty\{[RE_8O_{35}]^{46-}\}$ layers following similar linkages as in the A1-type structure. Six different lanthanide-oxygen polyhedra (*RE*1–*RE*4, *RE*6 and *RE*7) are in pairs of two forming five types of zigzag chains by edge-sharing, which propagate along the [010] direction ($4\times{}^1_\infty\{[RE_2O_{13}]^{20-}\}$ and $1\times{}^1_\infty\{[RE_2O_{12}]^{18-}\}$). They are then further condensed with each other via common vertices and edges to generate the basic layers of the A2-type structure. Eventually, the last two polyhedra $[(RE5)O_8]^{13-}$ and $[(RE8)O_7]^{11-}$ are grafted from above and below to these basic layers by sharing common edges and faces to form the corrugated $^2_\infty\{[RE_8O_{35}]^{46-}\}$ profile layers parallel to the (001) plane (Figure 7, *left*). These $^2_\infty\{[RE_8O_{35}]^{46-}\}$ layers are stacked along the crystallographic *c*-axis, again following a lock-and-key principle, and the atoms in each layer are related to those above and below by a *c*-glide plane (Figure 7, *bottom*

Table 1. Crystallographic data for the rare-earth metal(III) oxotellurates(IV) $RE_2Te_3O_9$ (RE = La and Ce).

Compound		$La_2Te_3O_9$	$Ce_2Te_3O_9$
Structure type		A1-type	A1-type
Crystal system		monoclinic	monoclinic
Space group		$P2_1$ (no. 4)	$P2_1$ (no. 4)
Unit-cell parameters,	a/pm	569.54(3)	567.02(3)
	b/pm	2230.12(13)	2222.61(13)
	c/pm	1464.71(9)	1457.13(9)
	β/°	101.205(3)	101.134(3)
Formula units per unit-cell (Z)		8	8
Calculated density (D_x in g/cm^3)		5.86	5.95
Molar volume (V_m in cm^3/mol)		137.38	135.64
Diffractometer, radiation		κ-CCD (Fa. Nonius), Mo-$K\alpha$: λ = 71.07 pm	
Index range ($\pm h_{max}/\pm k_{max}/\pm l_{max}$)		7/29/19	7/33/22
$2\theta_{max}$ (in °)		56.58	65.48
F(000)		2736	2752
Absorption correction		Program X-SHAPE[51]	
Absorption coefficient (μ in mm^{-1})		18.66	19.52
Extinction (g)		0.00006(2)	0.00114(2)
Collected reflections		29098	26006
Unique reflections		8527	10880
R_{int}/R_σ		0.098/0.076	0.114/0.085
Reflections with $\lvert F_o\rvert \geq 4\sigma(F_o)$		7083	5207
Structure solution and refinement		Programs SHELXS-97 and SHELXL-97[52]	
Scattering factors		International Tables, Vol. C[53]	
R_1/R_1 with $\lvert F_o\rvert \geq 4\sigma(F_o)$		0.075/0.056	0.130/0.051
wR_2 (for all reflections)		0.122	0.111
Flack x parameter		0.1605(6)	−0.0261(5)
BASF[a)]		0.27(2)	–
Goodness of Fit (GooF)		1.037	0.767
Residual electron density (max./min.) (ρ in e$^-\cdot 10^6$ pm^{-3})		4.28/−5.09	2.96/−3.81
CSD number		2036814	2036815

a) The batch scale factor is a refinement instruction for SHELXL-97[54], when twin domains are considered. The number represents the percental value of the second domain.

Table 2. Crystallographic data for the rare-earth metal(III) oxotellurates(IV) $RE_2Te_3O_9$ (RE = Pr and Nd).

Compound		$Pr_2Te_3O_9$	$Nd_2Te_3O_9$
Structure type		A2-type	A2-type
Crystal system		monoclinic	monoclinic
Space group		Cc (no. 9)	Cc (no. 9)
Unit-cell parameters,	a/pm	2838.61(16)	2826.38(16)
	b/pm	563.89(3)	561.47(3)
	c/pm	2522.08(15)	2511.94(15)
	β/°	118.816(3)	118.841(3)
Formula units per unit-cell (Z)		16	16
Calculated density (D_x in g/cm^3)		6.07	6.20
Molar volume (V_m in cm^3/mol)		133.21	131.50
Diffractometer, radiation		κ-CCD (Fa. Nonius), Mo-$K\alpha$: λ = 71.07 pm	
Index range ($\pm h_{max}/\pm k_{max}/\pm l_{max}$)		37/7/33	37/7/33
$2\theta_{max}$ (in °)		56.66	56.70
F(000)		5536	5568
Absorption correction		Program X-SHAPE[51]	
Absorption coefficient (μ in mm^{-1})		20.62	21.62
Extinction (g)		0.00009(1)	0.00006(3)
Collected reflections		33246	53831
Unique reflections		7920	8572
R_{int}/R_σ		0.124/0.085	0.117/0.068
Reflections with $\lvert F_o\rvert \geq 4\sigma(F_o)$		6680	7550
Structure solution and refinement		Programs SHELXS-97 and SHELXL-97[52]	
Scattering factors		International Tables, Vol. C[53]	
R_1/R_1 with $\lvert F_o\rvert \geq 4\sigma(F_o)$		0.077/0.062	0.051/0.041
wR_2 (for all reflections)		0.155	0.086
Flack x parameter		0.0009(2)	0.0000(2)
BASF[a)]		0.42(3)	0.14(2)
Goodness of Fit (GooF)		1.037	0.767
Residual electron density (max./min.) (ρ in e$^-\cdot 10^6$ pm^{-3})		4.53/−4.12	2.01/−1. 86
CSD number		2036816	2036817

a) The batch scale factor is a refinement instruction for SHELXL-97[54], when twin domains are considered. The number represents the percental value of the second domain.

right). It is interesting to mention that both the A1-type and the A2-type $RE_2Te_3O_9$ representatives contain two sorts of alternating rare-earth metal-oxygen polyhedra fused to $^2_\infty\{[RE_8O_{35}]^{46-}\}$ layers: one (α-layers) can be seen as identical in shape for both structure types and the other (β-layers in the A1-type and γ-layers in the A2-type) are created by different symmetry operations, such as a 2_1 screw axis and a *c*-glide plane, respectively. The difference of both structure types becomes particularly evident, when looking at these $^2_\infty\{[RE_8O_{35}]^{46-}\}$ layers along the [001] direction in the A1-type and along the [100] direction in the A2-type structure. In the A1-type infinite channels can be observed, whereas in the A2-type these channels are blocked by their *C*-base-centered motifs (Figure 3, *top right*, *versus* Figure 7, *top right*).

In the oxotellurate(IV) partial structure of A2-type $RE_2Te_3O_9$, twelve crystallographically different Te^{4+} cations are sur-

Table 3. Fractional atomic coordinates and (equivalent) isotropic displacement parameters for A1-type $La_2Te_3O_9$; all atoms occupy the general sites 2*a*. $U = U_{eq}$ for La and Te, $U = U_{iso}$ for O.

Atom	*x/a*	*y/b*	*z/c*	*U*/pm²
La1	0.6688(3)	0.25000(8)	0.39640(12)	95(4)
La2	0.4843(3)	0.24760(8)	0.02954(12)	110(4)
La3	0.6348(3)	0.11812(8)	0.21411(12)	85(3)
La4	0.7543(3)	0.76292(8)	0.38305(12)	97(4)
La5	0.1514(3)	0.76164(8)	0.18569(12)	90(3)
La6	0.9905(3)	0.38945(8)	0.02734(12)	99(4)
La7	0.1762(3)	0.38898(8)	0.39899(12)	99(4)
La8	0.0908(3)	0.52405(8)	0.21438(12)	103(4)
Te1	0.9615(4)	0.26007(9)	0.21325(13)	96(3)
Te2	0.7194(4)	0.50509(9)	0.41217(13)	107(4)
Te3	0.6378(4)	0.64468(9)	0.19855(14)	103(4)
Te4	0.2778(4)	0.64235(9)	0.39855(14)	118(5)
Te5	0.0095(4)	0.14375(9)	0.01349(13)	85(4)
Te6	0.2262(4)	0.86973(9)	0.42103(13)	92(4)
Te7	0.5908(4)	0.87098(9)	0.15215(13)	102(4)
Te8	0.6657(4)	0.99382(9)	0.38605(14)	148(5)
Te9	0.0848(4)	0.99356(9)	0.19756(14)	127(5)
Te10	0.5206(4)	0.50783(9)	0.01860(14)	112(5)
Te11	0.4898(4)	0.37286(9)	0.21246(14)	113(4)
Te12	0.2197(4)	0.14071(9)	0.41066(14)	109(5)
O1	0.831(3)	0.3126(9)	0.1150(13)	111(44)
O2	0.646(3)	0.2324(8)	0.2152(12)	59(30)
O3	0.929(3)	0.3111(9)	0.3149(14)	109(44)
O4	0.475(3)	0.5313(9)	0.3229(14)	298(56)
O5	0.591(3)	0.4330(9)	0.4373(14)	216(49)
O6	0.909(3)	0.4691(9)	0.3348(14)	242(54)
O7	0.828(3)	0.7117(9)	0.2432(13)	217(50)
O8	0.829(3)	0.6073(9)	0.1232(14)	239(50)
O9	0.435(3)	0.6908(9)	0.1060(13)	140(43)
O10	0.031(3)	0.6027(8)	0.3246(12)	83(38)
O11	0.097(3)	0.6952(8)	0.4579(12)	101(39)
O12	0.384(3)	0.7007(9)	0.3177(13)	127(41)
O13	0.318(3)	0.1497(9)	0.0854(12)	112(40)
O14	0.943(3)	0.7193(8)	0.0376(12)	102(39)
O15	0.827(3)	0.1768(9)	0.0983(14)	171(46)
O16	0.077(3)	0.8192(9)	0.3237(14)	232(50)
O17	0.506(3)	0.8252(9)	0.4695(14)	219(48)
O18	0.944(3)	0.3294(8)	0.4970(13)	105(42)
O19	0.345(3)	0.8311(9)	0.0727(13)	137(44)
O20	0.538(3)	0.8211(8)	0.2502(12)	35(35)
O21	0.837(3)	0.8290(9)	0.1048(13)	133(43)
O22	0.570(3)	0.0425(9)	0.4691(14)	293(56)
O23	0.854(3)	0.0451(8)	0.3312(13)	126(44)
O24	0.909(3)	0.9516(9)	0.4679(14)	220(50)
O25	0.340(3)	0.0412(8)	0.2381(13)	159(46)
O26	0.882(3)	0.0494(9)	0.1317(14)	216(49)
O27	0.185(3)	0.9536(9)	0.0989(13)	123(42)
O28	0.344(3)	0.5334(9)	0.1022(14)	219(48)
O29	0.632(3)	0.9341(9)	0.0057(14)	203(47)
O30	0.792(3)	0.4723(9)	0.0987(14)	154(46)
O31	0.323(3)	0.3273(9)	0.1169(14)	149(45)
O32	0.430(3)	0.3279(9)	0.3118(13)	94(43)
O33	0.209(3)	0.4194(8)	0.2101(14)	211(43)
O34	0.423(3)	0.1592(9)	0.3310(14)	157(46)
O35	0.951(3)	0.1768(8)	0.3380(13)	118(41)
O36	0.337(3)	0.2092(9)	0.4785(14)	246(51)

Table 4. Fractional atomic coordinates and (equivalent) isotropic displacement parameters for A1-type $Ce_2Te_3O_9$; all atoms occupy the general sites 2*a*. $U = U_{eq}$ for Ce and Te, $U = U_{iso}$ for O.

Atom	*x/a*	*y/b*	*z/c*	*U*/pm²
Ce1	0.6705(3)	0.25000(7)	0.39695(13)	148(4)
Ce2	0.4862(3)	0.24780(7)	0.02972(13)	146(4)
Ce3	0.6331(3)	0.11889(7)	0.21440(13)	146(3)
Ce4	0.7552(3)	0.76260(7)	0.38285(13)	152(3)
Ce5	0.1515(3)	0.76166(7)	0.18551(13)	143(3)
Ce6	0.9921(3)	0.38887(7)	0.02812(13)	151(4)
Ce7	0.1757(3)	0.38834(7)	0.40018(13)	157(4)
Ce8	0.0912(3)	0.52269(7)	0.21488(13)	148(4)
Te1	0.9640(4)	0.25954(8)	0.21287(14)	143(3)
Te2	0.7191(4)	0.50494(8)	0.41230(15)	144(4)
Te3	0.6355(4)	0.64380(8)	0.19903(15)	143(4)
Te4	0.2767(4)	0.64183(8)	0.39777(14)	156(4)
Te5	0.0100(4)	0.14313(8)	0.01258(15)	143(4)
Te6	0.2285(4)	0.86936(8)	0.41977(14)	149(4)
Te7	0.5909(4)	0.87158(8)	0.15231(14)	145(3)
Te8	0.6646(4)	0.99347(8)	0.38534(15)	179(4)
Te9	0.0823(4)	0.99384(8)	0.19688(14)	152(5)
Te10	0.5207(4)	0.50802(8)	0.01869(15)	155(4)
Te11	0.4928(4)	0.37285(8)	0.21271(14)	155(4)
Te12	0.2188(4)	0.14056(8)	0.41187(15)	156(4)
O1	0.831(4)	0.3130(8)	0.1133(15)	162(40)
O2	0.644(4)	0.2325(7)	0.2161(14)	156(33)
O3	0.929(4)	0.3103(8)	0.3126(13)	134(38)
O4	0.463(4)	0.5312(8)	0.3213(15)	353(50)
O5	0.576(4)	0.4298(8)	0.4413(15)	278(45)
O6	0.916(4)	0.4685(8)	0.3305(14)	173(40)
O7	0.829(4)	0.7112(8)	0.2440(14)	214(39)
O8	0.835(4)	0.6066(7)	0.1227(13)	156(35)
O9	0.425(4)	0.6918(7)	0.1082(13)	156(35)
O10	0.024(4)	0.6049(7)	0.3234(13)	169(35)
O11	0.099(4)	0.6965(8)	0.4591(14)	186(37)
O12	0.378(4)	0.7019(8)	0.3155(14)	200(39)
O13	0.322(4)	0.1524(8)	0.0886(14)	220(41)
O14	0.939(3)	0.7188(7)	0.0386(13)	136(32)
O15	0.830(3)	0.1775(7)	0.0969(13)	123(33)
O16	0.075(4)	0.8177(7)	0.3230(13)	172(36)
O17	0.510(4)	0.8262(8)	0.4691(15)	204(39)
O18	0.945(3)	0.3294(7)	0.4993(13)	96(31)
O19	0.341(3)	0.8303(7)	0.0709(13)	96(31)
O20	0.529(3)	0.8208(7)	0.2542(13)	137(33)
O21	0.833(4)	0.8293(8)	0.1072(15)	218(40)
O22	0.578(4)	0.0451(8)	0.4715(15)	390(57)
O23	0.866(4)	0.0453(8)	0.3298(15)	232(42)
O24	0.902(4)	0.9490(8)	0.4655(15)	328(51)
O25	0.351(4)	0.0433(8)	0.2348(15)	423(60)
O26	0.875(4)	0.0493(8)	0.1270(14)	206(39)
O27	0.196(4)	0.9545(8)	0.1007(15)	212(40)
O28	0.347(4)	0.5355(8)	0.1079(15)	251(41)
O29	0.647(4)	0.9348(8)	0.0089(15)	242(40)
O30	0.788(4)	0.4700(8)	0.0995(14)	214(42)
O31	0.324(4)	0.3252(8)	0.1139(14)	144(38)
O32	0.422(4)	0.3247(8)	0.3142(15)	201(45)
O33	0.216(4)	0.4185(8)	0.2108(15)	251(42)
O34	0.436(4)	0.1588(8)	0.3354(15)	264(49)
O35	0.951(4)	0.1761(8)	0.3351(14)	177(37)
O36	0.342(4)	0.2101(8)	0.4832(14)	210(39)

rounded by oxygen atoms, comprising the coordination numbers of C.N. = 3 + 2 (Te1–Te5) and C.N. = 3 + 1 (Te6–Te12). Apart from the three oxygen atoms, for which the bonds have a higher covalent character (d(Te–O) = 181–192 pm) within their

Table 5. Fractional atomic coordinates and (equivalent) isotropic displacement parameters for A2-type $Pr_2Te_3O_9$; all atoms occupy the general sites 4*a*. $U = U_{eq}$ for Pr and Te, $U = U_{iso}$ for O.

Atom	*x/a*	*y/b*	*z/c*	*U*/pm²
Pr1	0.25000(6)	0.0257(2)	0.25000(7)	104(3)
Pr2	0.43254(6)	0.0323(2)	0.24666(7)	92(3)
Pr3	0.64543(6)	0.0636(2)	0.26279(7)	103(3)
Pr4	0.04596(6)	0.0612(2)	0.26067(7)	88(3)
Pr5	0.28512(6)	0.0267(2)	0.61902(7)	96(3)
Pr6	0.80839(6)	0.0210(2)	0.38912(7)	99(3)
Pr7	0.99368(6)	0.0254(2)	0.38596(7)	91(3)
Pr8	0.95879(6)	0.0169(2)	0.52148(7)	97(3)
Te1	0.84607(7)	0.1427(3)	0.25917(8)	81(3)
Te2	0.57627(7)	0.0167(3)	0.36980(8)	90(3)
Te3	0.50272(7)	0.0403(3)	0.14325(8)	98(4)
Te4	0.54964(7)	0.0148(3)	0.00447(8)	97(4)
Te5	0.10153(7)	0.0765(3)	0.14171(8)	109(4)
Te6	0.89584(7)	0.0015(3)	0.64230(8)	89(4)
Te7	0.20937(7)	0.0167(3)	0.36994(8)	90(4)
Te8	0.14626(7)	0.0277(3)	0.99259(8)	135(4)
Te9	0.74044(7)	0.0174(3)	0.99374(8)	109(4)
Te10	0.35383(7)	0.0122(3)	0.00711(8)	103(4)
Te11	0.39491(7)	0.1141(3)	0.37183(8)	94(3)
Te12	0.69568(7)	0.0153(3)	0.64114(8)	102(4)
O1	0.9185(6)	0.233(3)	0.3127(8)	118(35)
O2	0.3336(7)	0.036(3)	0.7346(8)	142(35)
O3	0.8167(7)	0.220(3)	0.3110(8)	140(36)
O4	0.0338(6)	0.215(3)	0.8265(8)	118(34)
O5	0.5171(6)	0.189(3)	0.8263(8)	143(36)
O6	0.6046(6)	0.094(3)	0.8203(7)	140(35)
O7	0.9497(7)	0.225(3)	0.6038(8)	158(37)
O8	0.5542(7)	0.212(3)	0.2114(8)	153(36)
O9	0.4774(7)	0.124(3)	0.6905(8)	160(37)
O10	0.5168(7)	0.194(3)	0.5327(8)	173(38)
O11	0.5301(7)	0.137(3)	0.4302(8)	200(39)
O12	0.4937(7)	0.245(3)	0.9673(8)	236(44)
O13	0.0459(7)	0.147(3)	0.6014(8)	176(38)
O14	0.1551(6)	0.136(3)	0.6947(7)	120(34)
O15	0.0840(7)	0.214(3)	0.1976(8)	164(38)
O16	0.3621(6)	0.225(3)	0.1515(7)	121(34)
O17	0.9548(6)	0.077(3)	0.7180(7)	127(34)
O18	0.8700(6)	0.228(3)	0.1771(7)	141(36)
O19	0.7154(6)	0.222(3)	0.8250(7)	92(32)
O20	0.2327(6)	0.202(3)	0.8307(7)	72(32)
O21	0.1386(6)	0.089(3)	0.8184(8)	163(37)
O22	0.1271(7)	0.172(3)	0.0458(8)	235(43)
O23	0.1947(7)	0.192(3)	0.5464(8)	151(37)
O24	0.0849(7)	0.164(3)	0.4477(8)	227(42)
O25	0.7429(7)	0.225(3)	0.5436(8)	204(41)
O26	0.7725(7)	0.139(3)	0.4542(8)	173(37)
O27	0.7978(7)	0.194(3)	0.0485(8)	225(43)
O28	0.4095(7)	0.204(3)	0.5335(8)	197(39)
O29	0.3064(6)	0.139(3)	0.4325(7)	141(35)
O30	0.3788(6)	0.235(3)	0.9687(7)	105(34)
O31	0.4241(6)	0.240(3)	0.3253(7)	96(34)
O32	0.3245(7)	0.231(3)	0.3276(8)	146(38)
O33	0.9124(6)	0.111(3)	0.9176(7)	139(35)
O34	0.7486(7)	0.216(3)	0.1779(8)	174(38)
O35	0.2425(7)	0.241(3)	0.1581(8)	215(41)
O36	0.6910(7)	0.102(3)	0.7109(8)	233(42)

Table 6. Fractional atomic coordinates and (equivalent) isotropic displacement parameters for A2-type $Nd_2Te_3O_9$; all atoms occupy the general sites 4*a*. $U = U_{eq}$ for Pr and Te, $U = U_{iso}$ for O.

Atom	*x/a*	*y/b*	*z/c*	*U*/pm²
Nd1	0.25000(4)	0.02499(15)	0.25000(4)	103(2)
Nd2	0.43186(4)	0.03259(15)	0.24621(4)	104(2)
Nd3	0.64507(4)	0.06428(15)	0.26314(4)	98(2)
Nd4	0.04566(4)	0.06184(15)	0.26073(4)	910(2)
Nd5	0.28465(4)	0.02607(15)	0.61906(4)	95(18)
Nd6	0.80829(4)	0.02081(15)	0.38882(4)	101(2)
Nd7	0.99326(4)	0.02694(15)	0.38528(4)	97(2)
Nd8	0.95843(4)	0.01716(15)	0.52074(4)	95(2)
Te1	0.84582(5)	0.14302(17)	0.25895(5)	89(2)
Te2	0.57619(5)	0.01846(17)	0.36982(5)	86(2)
Te3	0.50284(5)	0.03934(18)	0.14319(5)	89(2)
Te4	0.54959(5)	0.01434(18)	0.00419(5)	94(2)
Te5	0.10152(5)	0.07775(18)	0.14185(5)	97(2)
Te6	0.89566(5)	0.00114(18)	0.64204(5)	88(2)
Te7	0.20928(5)	0.01685(17)	0.37017(5)	95(2)
Te8	0.14595(5)	0.02614(18)	0.99248(5)	125(2)
Te9	0.74028(5)	0.01809(18)	0.99358(5)	109(2)
Te10	0.35386(5)	0.01257(18)	0.00695(5)	99(2)
Te11	0.39438(5)	0.11478(18)	0.37117(5)	103(2)
Te12	0.69495(5)	0.01473(18)	0.64110(5)	95(2)
O1	0.9171(4)	0.2369(18)	0.3116(5)	117(22)
O2	0.3327(4)	0.0346(16)	0.7348(4)	104(19)
O3	0.8167(4)	0.2243(18)	0.3114(5)	133(22)
O4	0.0334(4)	0.2166(16)	0.8271(5)	129(21)
O5	0.5163(4)	0.1851(16)	0.8269(4)	69(20)
O6	0.6046(4)	0.0993(16)	0.8201(4)	125(21)
O7	0.9484(4)	0.2272(18)	0.6033(5)	143(22)
O8	0.5544(4)	0.2154(17)	0.2110(4)	107(21)
O9	0.4776(4)	0.1243(17)	0.6912(4)	118(21)
O10	0.5148(4)	0.1917(18)	0.5320(5)	226(25)
O11	0.5305(4)	0.1385(17)	0.4301(5)	155(22)
O12	0.4941(4)	0.2476(17)	0.9670(5)	121(22)
O13	0.0458(4)	0.1441(17)	0.6010(4)	115(21)
O14	0.1553(4)	0.1340(18)	0.6963(5)	161(22)
O15	0.0839(4)	0.2207(16)	0.1990(4)	88(20)
O16	0.3611(4)	0.2269(17)	0.1503(4)	133(21)
O17	0.9543(4)	0.0814(17)	0.7181(4)	127(21)
O18	0.8687(4)	0.2245(16)	0.1779(4)	86(20)
O19	0.7158(4)	0.2233(17)	0.8269(5)	148(22)
O20	0.2336(4)	0.1974(17)	0.8309(4)	106(21)
O21	0.1382(4)	0.0891(17)	0.8184(4)	127(21)
O22	0.1254(4)	0.1652(18)	0.0436(5)	283(28)
O23	0.1958(4)	0.1947(18)	0.5459(5)	185(24)
O24	0.0858(4)	0.1710(18)	0.4477(5)	188(24)
O25	0.7419(4)	0.2316(18)	0.5426(5)	207(25)
O26	0.7724(4)	0.1409(18)	0.4540(5)	179(23)
O27	0.7976(4)	0.1993(18)	0.0516(5)	158(23)
O28	0.4093(4)	0.2065(18)	0.5322(5)	178(23)
O29	0.3066(4)	0.1366(18)	0.4331(5)	165(22)
O30	0.3771(4)	0.2381(17)	0.9679(5)	112(21)
O31	0.4230(4)	0.2382(17)	0.3240(4)	96(21)
O32	0.3237(4)	0.2302(18)	0.3265(5)	110(22)
O33	0.9125(4)	0.1021(18)	0.9171(4)	146(22)
O34	0.7482(4)	0.2164(17)	0.1772(5)	131(21)
O35	0.2423(4)	0.2303(18)	0.1591(5)	151(23)
O36	0.6909(4)	0.1026(17)	0.7104(4)	141(22)

$[TeO_3]^{2-}$ ψ^1-tetrahedra, strong secondary $Te^{4+}\cdots O^{2-}$ contacts (d(Te···O) = 246–292 pm) also appear in the A2-type crystal structure of $Pr_2Te_3O_9$ and $Nd_2Te_3O_9$. All the oxotellurate(IV) units except for those containing Te12 are again alike in both cases

Table 7. Selected interatomic distances (*d*/pm) in A1-type $La_2Te_3O_9$. The standard deviations are typically ±0.3 pm.

La1–O32	239.6	La2–O31	247.0	La3–O13	244.6
–O3	248.0	–O9	247.3	–O34	245.0
–O34	254.0	–O14	252.1	–O25	247.2
–O35	255.3	–O15	256.0	–O23	251.4
–O36	259.0	–O1	257.0	–O26	254.0
–O11	259.0	–O13	257.6	–O2	254.8
–O18	262.1	–O19	268.5	–O15	255.0
–O2	266.0	–O2	271.8	–O35	264.2
···O17	290.0	···O21	301.7		
La4–O7	245.0	La5–O7	244.0	La6–O27	239.7
–O20	246.2	–O14	245.0	–O1	242.0
–O17	249.0	–O21	246.0	–O30	250.0
–O36	250.0	–O16	250.0	–O31	250.0
–O16	251.0	–O12	251.8	–O29	250.0
–O11	254.1	–O20	258.5	–O19	253.2
–O12	255.2	–O19	265.9	–O21	269.7
–O19	265.7	–O9	268.3	–O33	280.0
La7–O6	242.0	La8–O28	240.0		
–O3	242.0	–O33	243.4		
–O32	251.0	–O30	244.6		
–O18	251.2	–O4	245.0		
–O5	252.0	–O10	245.3		
–O24	252.0	–O6	253.0		
–O17	277.0	–O8	258.0		
–O33	289.0				
Te1–O1	189.2	Te2–O4	181.0	Te3–O7	188.0
–O2	190.7	–O5	183.0	–O8	189.0
–O3	191.0	–O6	189.0	–O9	190.3
···O15	252.0	···O24	274.6	···O12	277.1
···O35	261.4	···O22	274.8	···O10	277.3
Te4–O10	182.8	Te5–O13	186.9	Te6–O16	189.0
–O11	188.6	–O14	188.5	–O17	190.0
–O12	193.3	–O15	192.0	–O18	191.0
···O36	295.8	···O8	250.0	···O5	255.7
···O22	296.9				
Te7–O19	186.3	Te8–O22	179.0	Te9–O25	180.6
–O20	188.6	–O23	185.5	–O26	184.0
–O21	192.0	–O24	189.0	–O27	187.9
···O29	261.4	···O25	277.3	···O23	280.7
Te10–O28	182.0	Te11–O31	184.0	Te12–O34	184.0
–O29	186.0	–O32	185.2	–O35	186.7
–O30	192.0	–O33	190.1	–O36	187.0
···O27	289.1	···O1	294.9		

Table 8. Selected interatomic distances (*d*/pm) in A1-type $Ce_2Te_3O_9$. The standard deviations are typically ±0.3 pm.

Ce1–O32	235.0	Ce2–O31	240.0	Ce3–O25	238.0
–O3	248.0	–O9	249.5	–O13	240.0
–O34	250.0	–O14	250.6	–O34	243.0
–O11	254.0	–O13	253.0	–O2	252.7
–O35	256.7	–O15	254.4	–O23	253.0
–O36	260.0	–O1	255.0	–O26	256.0
–O18	262.0	–O19	265.1	–O15	257.3
–O2	263.9	–O2	271.0	–O35	259.0
···O17	291.0	···O21	302.3		
Ce4–O36	243.0	Ce5–O7	243.0	Ce6–O1	238.0
–O7	243.0	–O14	243.9	–O29	244.0
–O20	243.1	–O21	246.0	–O27	245.0
–O16	247.9	–O12	246.0	–O30	248.0
–O17	249.0	–O16	246.8	–O31	249.0
–O11	252.0	–O20	254.5	–O19	250.8
–O12	256.0	–O9	260.1	–O21	272.0
–O18	263.0	–O19	263.8	–O33	280.0
Ce7–O6	241.0	Ce8–O28	234.0		
–O5	242.0	–O4	237.0		
–O3	243.1	–O33	242.6		
–O24	249.0	–O6	243.0		
–O32	249.0	–O30	246.0		
–O18	250.0	–O10	249.4		
–O17	272.0	–O8	257.7		
–O33	289.0				
Te1–O3	188.1	Te2–O4	186.0	Te3–O7	189.8
–O1	191.0	–O5	194.0	–O8	191.9
–O2	192.0	–O6	196.0	–O9	192.4
···O15	250.2	···O22	275.7	···O10	271.0
···O35	258.2	···O24	280.3	···O12	276.3
Te4–O10	182.0	Te5–O14	188.6	Te6–O17	188.0
–O11	190.9	–O15	190.1	–O18	189.5
–O12	195.3	–O13	191.0	–O16	189.6
···O36	288.6	···O8	244.6	···O5	250.4
···O22	292.1				
Te7–O21	188.0	Te8–O22	184.0	Te9–O26	186.0
–O19	190.0	–O24	188.0	–O27	187.0
–O20	195.1	–O23	191.0	–O25	187.0
···O29	258.8	···O25	277.3	···O23	273.4
Te10–O28	188.0	Te11–O33	186.0	Te12–O34	186.0
–O29	188.9	–O31	189.0	–O35	188.0
–O30	193.0	–O32	193.0	–O36	191.8
···O27	284.6	···O1	293.6		

(A1- and A2-type). Unlike in the A1-type, Te12 in the A2-type structure contains one extra secondary contact to the oxygen atom O22 (*d*(Te12···O22) = 291 pm), through which along with other secondary bonding interactions (SBIs) (Figure 8) all twelve oxotellurate(IV) units are interconnected to $^1_\infty\{[Te_{12}O_{36}]^{24-}\}$ strands running along the [010] direction (Figure 9). In addition, O–Te–O angles from 84 to 105° (Tables 11–14) move the Te^{4+} cations out of their triangular (O,O,O)-plane by distances between 87 and 110 pm. The listed displacement parameters of the A2-type are in Tables 3–6.

Structure Comparison of the A1- and A2-Type

By comparing the complete crystal structures of A1-type and A2-type $RE_2Te_3O_9$ (*RE* = La–Nd), both $[(Te1)O_3]^{2-}$ and $[(Te11)O_3]^{2-}$ units reside within the channels of the porous $^2_\infty\{[RE_8O_{35}]^{46-}\}$ sheets. The stabilization of both structures is further ensured via three oxotellurate(IV) units in the A1-type (Te3, Te4 and Te8) and via four of them in the A2-type (Te3, Te5, Te8 and Te9), which are located in between the $^2_\infty\{[RE_8O_{35}]^{46-}\}$ layers. These aforementioned three (A1-type) and four units (A2-type) are

Table 9. Selected interatomic distances (*d*/pm) in A2-type $Pr_2Te_3O_9$. The standard deviations are typically ±0.3 pm.

Pr1–O32	237.7	Pr2–O31	241.1	Pr3–O8	242.0
–O3	247.3	–O9	247.9	–O6	242.0
–O34	250.6	–O18	248.6	–O36	242.6
–O35	253.1	–O17	249.3	–O19	245.1
–O14	253.2	–O16	251.1	–O21	247.1
–O36	256.9	–O1	253.3	–O14	252.2
–O2	260.7	–O5	259.0	–O20	259.3
–O20	264.5	–O2	270.2	–O15	262.1
···O19	288.8	···O4	296.1		
Pr4–O8	239.7	Pr5–O16	239.3	Pr6–O3	237.6
–O17	240.4	–O25	239.8	–O26	240.6
–O4	242.0	–O35	242.1	–O29	242.7
–O21	246.2	–O23	250.7	–O32	244.5
–O15	246.8	–O27	252.7	–O30	246.0
–O6	253.0	–O18	254.2	–O20	248.4
–O5	258.7	–O2	255.4	–O19	271.1
–O9	259.7	–O34	262.0	–O33	278.2
Pr7–O1	235.3	Pr8–O28	235.9		
–O24	242.1	–O10	238.0		
–O12	242.0	–O33	240.6		
–O31	243.5	–O13	243.2		
–O11	244.8	–O12	244.0		
–O5	250.2	–O30	244.3		
–O4	265.1	–O7	250.3		
–O33	288.6				
Te1–O2	189.4	Te2–O6	188.8	Te3–O7	188.7
–O1	190.7	–O5	189.7	–O8	190.0
–O3	190.9	–O4	191.4	–O9	190.3
···O18	251.6	···O11	253.4	···O13	264.1
···O34	256.2	···O24	272.2	···O15	274.6
Te4–O10	184.3	Te5–O15	187.4	Te6–O17	188.3
–O11	188.5	–O13	188.8	–O16	189.0
–O12	191.2	–O14	188.9	–O18	189.7
···O22	272.9	···O22	289.2	···O7	251.1
···O24	277.7	···O36	291.7		
Te7–O21	188.8	Te8–O22	186.1	Te9–O25	183.6
–O20	189.1	–O23	186.4	–O26	184.1
–O19	191.6	–O24	189.4	–O27	186.4
···O29	252.4	···O25	278.0	···O23	279.2
Te10–O28	184.9	Te11–O33	185.3	Te12–O35	181.5
–O29	190.8	–O31	187.2	–O34	186.5
–O30	192.0	–O32	187.6	–O36	189.0
···O26	283.0	···O1	287.3	···O22	285.9

Table 10. Selected interatomic distances (*d*/pm) in A2-type $Nd_2Te_3O_9$. The standard deviations are typically ±0.3 pm.

Nd1–O32	234.5	Nd2–O31	238.4	Nd3–O8	240.2
–O3	244.4	–O17	245.6	–O6	240.5
–O35	247.2	–O9	246.6	–O36	244.3
–O34	250.3	–O18	248.4	–O21	245.3
–O14	250.9	–O1	250.8	–O19	246.6
–O36	255.9	–O16	251.9	–O14	249.8
–O2	256.4	–O5	257.4	–O15	257.3
–O20	261.0	–O2	270.4	–O20	261.6
···O19	290.9	···O4	295.3		
Nd4–O8	238.8	Nd5–O25	237.6	Nd6–O3	236.5
–O17	240.7	–O16	238.1	–O26	240.0
–O4	243.0	–O35	238.3	–O30	241.6
–O15	244.5	–O27	244.6	–O29	243.8
–O21	244.9	–O23	247.5	–O32	244.3
–O6	249.5	–O18	252.9	–O20	247.2
–O9	257.2	–O2	254.8	–O19	268.5
–O5	260.8	–O34	259.4	–O33	276.4
Nd7–O1	236.8	Nd8–O28	233.4		
–O12	240.2	–O10	235.0		
–O11	244.7	–O33	237.7		
–O31	244.8	–O13	242.3		
–O24	244.8	–O12	242.7		
–O5	247.2	–O30	244.7		
–O4	262.5	–O7	251.7		
–O33	285.2				
Te1–O1	187.4	Te2–O4	189.1	Te3–O7	189.7
–O2	188.8	–O5	189.1	–O8	189.9
–O3	191.5	–O6	189.9	–O9	190.8
···O18	245.7	···O11	251.1	···O13	264.4
···O34	255.5	···O24	268.3	···O15	270.5
Te4–O10	185.9	Te5–O13	187.7	Te6–O16	187.6
–O11	187.7	–O14	189.5	–O17	188.3
–O12	190.7	–O15	191.0	–O18	191.4
···O22	271.4	···O36	289.3	···O7	248.7
···O24	275.4	···O22	289.3		
Te7–O19	188.1	Te8–O22	182.2	Te9–O25	185.1
–O20	188.3	–O23	187.1	–O26	186.7
–O21	188.7	–O24	188.1	–O27	187.3
···O29	251.4	···O25	281.8	···O23	273.9
Te10–O28	184.6	Te11–O31	186.1	Te12–O34	185.9
–O29	188.1	–O32	187.2	–O35	186.0
–O30	190.3	–O33	188.4	–O36	186.6
···O26	281.1	···O1	284.3	···O22	290.6

involved in the cohesion of both layers (A1-type: α and β, A2-type: α and γ). Finally the twelve oxotellurate(IV) units interconnect the surface network $^{2}_{\infty}\{[RE_2O_9]^{12-}\}$ to form an electroneutral three-dimensional crystal structure. Within and in between those porous layers, there is still enough space left to accommodate the stereochemically active lone-pair electrons at each Te^{4+} cation. In both the A1-type and the A2-type structure, one can always observe different symmetry elements working on their atoms, for example Te1 and Te11 in the A1-type are related to their equivalents in the next layer by a twofold rotation around the *b*-axis, whereas in the A2-type Te1 and Te11 are mirror-related to their counterparts in the neighboring layer through the (010) plane (Figure 10).

Worth noticing is, that in the A-type, the B-type[33–36] and C-type[33–35,37,38] structures for the composition $RE_2Te_3O_9$, always one single oxygen atom (O22 in both A-types, O13 in the B-type, and O8 in the C-type) is not part of the rare-earth metal coordination spheres, but only attached to the Te^{4+} cations. For $La_2Te_3O_9$ and $Nd_2Te_3O_9$, O22 is covalently bonded to Te8 and weakly attached to Te2 and Te4 in the A1-type through

Table 11. Important angles (∢/°) in A1-type $La_2Te_3O_9$. The standard deviations are typically ±0.9°.

A1-type $La_2Te_3O_9$			
O1–Te1–O2	88.9	O4–Te2–O5	98.5
O1–Te1–O3	98.1	O4–Te2–O6	98.7
O2–Te1–O3	87.0	O5–Te2–O6	92.6
O15–Te1–O1	85.7	O24–Te2–O4	172.0
O15–Te1–O2	66.8	O24–Te2–O5	77.2
O15–Te1–O3	153.5	O24–Te2–O6	74.9
O15–Te1–O35	84.2	O24–Te2–O22	102.1
O35–Te1–O1	155.9	O22–Te2–O4	83.5
O35–Te1–O2	67.0	O22–Te2–O5	80.1
O35–Te1–O3	81.9	O22–Te2–O6	172.5
O7–Te3–O8	101.3	O10–Te4–O11	98.6
O7–Te3–O9	92.7	O10–Te4–O12	104.9
O8–Te3–O9	99.3	O11–Te4–O12	97.2
O12–Te3–O7	76.1	O36–Te4–O10	177.7
O12–Te3–O8	176.3	O36–Te4–O11	79.1
O12–Te3–O9	83.5	O36–Te4–O12	75.5
O12–Te3–O10	100.7	O36–Te4–O22	83.8
O10–Te3–O7	72.6	O22–Te4–O10	96.7
O10–Te3–O8	76.0	O22–Te4–O11	106.5
O10–Te3–O9	163.0	O22–Te4–O12	144.9
O13–Te5–O14	88.2	O16–Te6–O17	101.2
O13–Te5–O15	100.2	O16–Te6–O18	89.1
O14–Te5–O15	93.0	O17–Te6–O18	90.7
O8–Te5–O13	91.3	O5–Te6–O16	174.9
O8–Te5–O14	82.5	O5–Te6–O17	78.8
O8–Te5–O15	167.5	O5–Te6–O18	85.8
O19–Te7–O20	89.0	O22–Te8–O23	101.5
O19–Te7–O21	93.0	O22–Te8–O24	98.8
O20–Te7–O21	102.9	O23–Te8–O24	99.7
O29–Te7–O19	85.5	O25–Te8–O22	93.1
O29–Te7–O20	174.4	O25–Te8–O23	77.4
O29–Te7–O21	77.2	O25–Te8–O24	168.1
O25–Te9–O26	99.0	O28–Te10–O29	96.2
O25–Te9–O27	100.7	O28–Te10–O30	101.6
O26–Te9–O27	99.9	O29–Te10–O30	92.4
O23–Te9–O25	89.2	O27–Te10–O28	172.5
O23–Te9–O26	75.9	O27–Te10–O29	79.6
O23–Te9–O27	169.8	O27–Te10–O30	72.5
O31–Te11–O32	98.7	O34–Te12–O35	95.1
O31–Te11–O33	88.7	O34–Te12–O36	87.1
O32–Te11–O33	91.6	O35–Te12–O36	96.9
O1–Te11–O31	70.8		
O1–Te11–O32	111.9		
O1–Te11–O33	150.6		

Table 12. Important angles (∢/°) in A1-type $Ce_2Te_3O_9$. The standard deviations are typically ±0.9°.

A1-type $Ce_2Te_3O_9$			
O1–Te1–O2	88.7	O4–Te2–O5	97.1
O1–Te1–O3	97.4	O4–Te2–O6	98.8
O2–Te1–O3	85.8	O5–Te2–O6	95.0
O15–Te1–O1	85.2	O22–Te2–O4	81.4
O15–Te1–O2	67.9	O22–Te2–O5	79.3
O15–Te1–O3	153.6	O22–Te2–O6	174.3
O15–Te1–O35	84.1	O22–Te2–O24	103.8
O35–Te1–O1	155.4	O24–Te2–O4	171.4
O35–Te1–O2	66.8	O24–Te2–O5	77.4
O35–Te1–O3	82.9	O24–Te2–O6	75.3
O7–Te3–O8	100.0	O10–Te4–O11	98.0
O7–Te3–O9	92.3	O10–Te4–O12	103.5
O8–Te3–O9	101.3	O11–Te4–O12	95.5
O10–Te3–O7	71.3	O22–Te4–O10	98.6
O10–Te3–O8	75.9	O22–Te4–O11	106.0
O10–Te3–O9	162.3	O22–Te4–O12	146.5
O10–Te3–O12	101.3	O22–Te4–O36	84.9
O12–Te3–O7	76.0	O36–Te4–O10	175.2
O12–Te3–O8	175.8	O36–Te4–O11	77.8
O12–Te3–O9	80.3	O36–Te4–O12	74.8
O13–Te5–O14	86.3	O16–Te6–O17	102.1
O13–Te5–O15	97.7	O16–Te6–O18	87.6
O14–Te5–O15	92.3	O17–Te6–O18	91.5
O8–Te5–O13	93.8	O5–Te6–O16	174.4
O8–Te5–O14	82.6	O5–Te6–O17	75.8
O8–Te5–O15	167.0	O5–Te6–O18	87.2
O19–Te7–O20	88.4	O22–Te8–O23	100.0
O19–Te7–O21	92.7	O22–Te8–O24	99.1
O20–Te7–O21	103.2	O23–Te8–O24	99.6
O29–Te7–O19	87.2	O25–Te8–O22	94.4
O29–Te7–O20	175.7	O25–Te8–O23	76.6
O29–Te7–O21	77.2	O25–Te8–O24	166.5
O25–Te9–O26	99.4	O28–Te10–O29	96.8
O25–Te9–O27	96.8	O28–Te10–O30	100.1
O26–Te9–O27	99.8	O29–Te10–O30	93.2
O23–Te9–O25	89.8	O27–Te10–O28	172.9
O23–Te9–O26	77.8	O27–Te10–O29	80.2
O23–Te9–O27	173.4	O27–Te10–O30	73.7
O31–Te11–O32	97.1	O34–Te12–O35	96.0
O31–Te11–O33	89.6	O34–Te12–O36	86.3
O32–Te11–O33	90.8	O35–Te12–O36	98.7
O1–Te11–O31	69.7		
O1–Te11–O32	112.3		
O1–Te11–O33	150.2		

secondary contacts (C.N. = 1 + 2). For the A2-type structure, O22 is weakly bonded to Te4, Te5 and Te12 via secondary contacts (C.N. = 1 + 3) additional to the covalent Te8–O22 bond.

Secondary Bonding Interactions

The definition of secondary bonding interactions (SBIs) was established by *Alcock et al.* putting the theory forward that in several cases intramolecular distances occur, which are longer than normal bond lengths and in contrast, intermolecular distances were discovered that are shorter than *van der Waals* distances (for Te···O: 358 pm).[41] In addition, an approximately linear arrangement was found between halogens and O, S, Se or N. The definition of the secondary bond was made by the assumption that *Y*–*A* (*A* = central atom, *Y* = atom bonded to *A*) is a normal or primary bond and *A*···*X* (*X* = outer atom) is the short intermolecular distance with such a linear *Y*–*A*···*X* arrange-

Table 13. Important angles (∢/°) in A2-type $Pr_2Te_3O_9$. The standard deviations are typically ±0.9°.

A2-type $Pr_2Te_3O_9$			
O1–Te1–O2	86.7	O4–Te2–O5	90.9
O1–Te1–O3	97.5	O4–Te2–O6	103.7
O2–Te1–O3	86.1	O5–Te2–O6	87.4
O18–Te1–O1	84.6	O11–Te2–O4	76.4
O18–Te1–O2	68.3	O11–Te2–O5	86.7
O18–Te1–O3	154.1	O11–Te2–O6	174.1
O18–Te1–O34	85.8	O11–Te2–O24	69.8
O34–Te1–O1	154.7	O24–Te2–O4	143.3
O34–Te1–O2	70.0	O24–Te2–O5	73.6
O34–Te1–O3	81.4	O24–Te2–O6	108.5
O7–Te3–O8	100.9	O10–Te4–O11	97.6
O7–Te3–O9	103.1	O10–Te4–O12	99.7
O8–Te3–O9	92.3	O11–Te4–O12	92.6
O13–Te3–O7	74.2	O22–Te4–O10	82.2
O13–Te3–O8	73.6	O22–Te4–O11	81.7
O13–Te3–O9	164.5	O22–Te4–O12	174.1
O13–Te3–O15	101.9	O22–Te4–O24	103.6
O15–Te3–O7	176.1	O24–Te4–O10	171.9
O15–Te3–O8	78.2	O24–Te4–O11	77.9
O15–Te3–O9	80.9	O24–Te4–O12	74.0
O13–Te5–O14	97.9	O16–Te6–O17	86.9
O13–Te5–O15	103.0	O16–Te6–O18	99.7
O14–Te5–O15	98.4	O17–Te6–O18	92.2
O22–Te5–O13	99.0	O7–Te6–O16	94.4
O22–Te5–O14	105.6	O7–Te6–O17	82.5
O22–Te5–O15	144.8	O7–Te6–O18	164.7
O22–Te5–O36	83.5		
O36–Te5–O13	176.0		
O36–Te5–O14	78.4		
O36–Te5–O15	76.3		
O19–Te7–O20	92.1	O22–Te8–O23	97.8
O19–Te7–O21	101.8	O22–Te8–O24	100.3
O20–Te7–O21	87.6	O23–Te8–O24	101.4
O29–Te7–O19	77.1	O25–Te8–O22	90.8
O29–Te7–O20	87.3	O25–Te8–O23	77.2
O29–Te7–O21	174.8	O25–Te8–O24	169.1
O25–Te9–O26	98.5	O28–Te10–O29	97.7
O25–Te9–O27	99.3	O28–Te10–O30	98.9
O26–Te9–O27	100.1	O29–Te10–O30	92.9
O23–Te9–O25	89.1	O26–Te10–O28	172.0
O23–Te9–O26	172.2	O26–Te10–O29	79.5
O23–Te9–O27	76.8	O26–Te10–O30	73.9
O31–Te11–O32	99.3	O34–Te12–O35	95.2
O31–Te11–O33	90.5	O34–Te12–O36	96.8
O32–Te11–O33	88.0	O35–Te12–O36	87.5
O1–Te11–O31	71.0	O22–Te12–O34	155.4
O1–Te11–O32	113.7	O22–Te12–O35	81.7
O1–Te11–O33	152.9	O22–Te12–O36	107.4

Table 14. Important angles (∢/°) in A2-type $Nd_2Te_3O_9$. The standard deviations are typically ±0.9°.

A2-type $Nd_2Te_3O_9$			
O1–Te1–O2	86.3	O4–Te2–O5	90.0
O1–Te1–O3	96.9	O4–Te2–O6	105.0
O2–Te1–O3	84.8	O5–Te2–O6	87.7
O18–Te1–O1	84.8	O11–Te2–O4	75.9
O18–Te1–O2	69.2	O11–Te2–O5	85.8
O18–Te1–O3	153.8	O11–Te2–O6	173.5
O18–Te1–O34	85.3	O11–Te2–O24	69.9
O34–Te1–O1	153.8	O24–Te2–O4	143.0
O34–Te1–O2	67.6	O24–Te2–O5	74.0
O34–Te1–O3	81.9	O24–Te2–O6	107.5
O7–Te3–O8	100.9	O10–Te4–O11	97.8
O7–Te3–O9	102.2	O10–Te4–O12	98.7
O8–Te3–O9	92.5	O11–Te4–O12	93.0
O13–Te3–O7	74.7	O22–Te4–O10	83.2
O13–Te3–O8	73.0	O22–Te4–O11	80.2
O13–Te3–O9	164.0	O22–Te4–O12	173.2
O13–Te3–O15	102.4	O22–Te4–O24	103.1
O15–Te3–O7	177.1	O24–Te4–O10	171.2
O15–Te3–O8	77.7	O24–Te4–O11	77.5
O15–Te3–O9	80.5	O24–Te4–O12	74.3
O13–Te5–O14	98.5	O16–Te6–O17	86.8
O13–Te5–O15	103.6	O16–Te6–O18	98.0
O14–Te5–O15	97.5	O17–Te6–O18	92.1
O36–Te5–O13	176.5	O7–Te6–O16	94.0
O36–Te5–O14	78.1	O7–Te6–O17	82.8
O36–Te5–O15	76.2	O7–Te6–O18	166.6
O36–Te5–O22	84.6		
O22–Te5–O13	97.2		
O22–Te5–O14	106.6		
O22–Te5–O15	145.3		
O19–Te7–O20	91.7	O22–Te8–O23	99.5
O19–Te7–O21	102.4	O22–Te8–O24	99.8
O20–Te7–O21	88.6	O23–Te8–O24	101.0
O29–Te7–O19	76.9	O25–Te8–O22	92.6
O29–Te7–O20	86.3	O25–Te8–O23	76.3
O29–Te7–O21	174.7	O25–Te8–O24	167.6
O25–Te9–O26	97.4	O28–Te10–O29	97.1
O25–Te9–O27	99.2	O28–Te10–O30	100.0
O26–Te9–O27	102.3	O29–Te10–O30	92.6
O23–Te9–O25	89.8	O26–Te10–O28	171.5
O23–Te9–O26	172.5	O26–Te10–O29	79.1
O23–Te9–O27	74.4	O26–Te10–O30	72.7
O31–Te11–O32	98.9	O34–Te12–O35	95.8
O31–Te11–O33	90.2	O34–Te12–O36	97.4
O32–Te11–O33	88.4	O35–Te12–O36	86.0
O1–Te11–O31	70.4	O22–Te12–O34	154.4
O1–Te11–O32	112.9	O22–Te12–O35	81.0
O1–Te11–O33	152.7	O22–Te12–O36	107.6

ment. The resulting geometries of linear interactions were found to be a line, a square, a trigonal bipyramid and an octahedron. For the resulting geometries three rules have been established. The first one that primary bonds to the central atom are governed by an amount of lone and bonded electron pairs in the usual geometry. The second one is describing that secondary bonds can be formed linear in any direction with primary bonds. The last one has the crucial point that secondary bonds can not be formed in the direction to the lone pair of the central atom.[41]

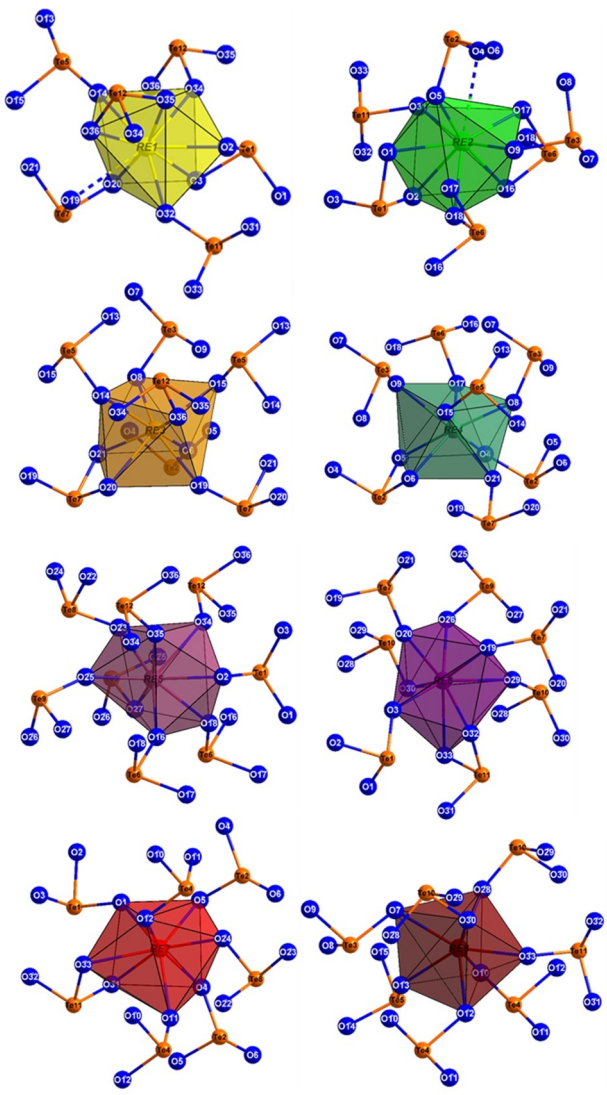

Figure 6. Oxygen coordination polyhedra of the eight crystallographically independent RE^{3+} cations (RE = Pr and Nd) in the A2-type crystal structure for the composition $RE_2Te_3O_9$ along with the attached ψ^1-tetrahedral $[TeO_3]^{2-}$ anions.

Among other things it was established that the strength of secondary bonds is affected by electronegativity. When *A* becomes less electronegative the interaction will be stronger, assuming that not an electrostatic attraction is responsible, but a "dative interaction". Such a "dative interaction" (nowadays known as hyperconjugation) is described by the interaction between a lone pair from *X* and an empty orbital of *A*. The empty orbital is the σ*-orbital of the primary bond. This σ*-orbital is expected to reach further in space directing away from *Y*. The hyperconjugation results in a weak bond. Two trends were suggested for the strength of secondary bonds. The first one affects *A*, for when its electronegativity is decreasing the results are less compact anti-bonding orbitals, leading to a better overlap with the lone-pair orbital of *X*. The second one is *vice versa*, for when the electronegativity of *X* is decreasing, the lone-pair orbital will also be less compact and a better overlap should be the result.[41]

The new compounds $RE_2Te_3O_9$ with the A1-type and A2-type structure can be slotted into the category "structures with monomeric $[(Te^{4+})(O^{2-})_3]$ units and no larger structural unit, but with additional anions or water" by *Christy et al.*[42] due to the mentioned rather weak secondary bonding interactions (SBIs) within this article.

The chosen rules for the secondary bonds are subdivided in own constructed points. Every structure defines its own threshold, of course Thus there can not be three secondary bonds, assuming that the lone pair at the Te^{4+} cation is blocking the equatorial position for another oxygen atom. There are only two possible ideal geometries, which can be achieved by SBIs for Te···O contacts. These are the ψ^1-trigonal bipyramidal and the ψ^1-octahedral coordination.[43,44] Two SBIs have a similar distance, due to target a ψ^1-octahedron. An octahedral coordination is known for its equidistant separations. The last rule contains the general threshold, which lies in the range from 208 to 298 pm according to *Zemann et al.*[7] The different features for SBIs are described by *Cozzolino et al.*.[45] The condition is, that a heavy group p-block element is bonded to a more electronegative atom. The overlap of the σ*-Te–O molecular orbital with a non-bonding p-orbital from another oxygen atom generates the secondary bonding interaction (SBI or hyperconjugation), which can be seen in Figure 11. Another name for this specific interaction between tellurium and oxygen is called "chalcogen bonding".[46] A σ-hole interaction must not considered, since hyperconjugation should more stable than the electrostatic effect. The other reason is, that SBIs have more covalent character, but lighter chalcogens like oxygen or sulfur tend to interact with σ-holes, whereas heavier chalcogen atoms like tellurium are more prone to hyperconjugation. For σ-hole interactions like S···O and S···S, the electrostatic effect is decreasing due to less electronegativity of the outer atom, while the hyperconjugation for Te···O and Te···S increases due to better overlap.[47] If the chalcogen has more substituents, more σ-holes are generated.[48]

On the note of coordination, the description of the Te^{4+} cations as 3, 3 + 1 and 3 + 2 is accurate, but some of these longer bonds ($d \approx 250$ pm) are on the same side of these tellurium(IV) centers as the short primary bonds ($d < 200$ pm), which suits well in a simple electrostatic model. Others with $d >$ 270 pm can be found on the same side as the stereochemically active lone pair at these Te^{4+} cations being more reasonable explained by an orbital model by *Alcock et al.*.[41] The range 250–300 pm[7,33] is not free from arbitrariness, but if farther apart oxygen atoms with distances from 300–350 pm would be included, those could even be discussed as more distant secondary bonds tending to bring the overall coordination number for all Te^{4+} cations under consideration from C.N. = 3, 3 + 1 or 3 + 2 to C.N. = 3 + 3–3 + 9 and to complicate the structure description unnecessarily. Sometimes those bonds with $d >$ 300 pm are also present at the same side of the Te^{4+} cations as the three short primary bonds, not showing up in any of the figures (Figures 4 and 8), but still contributing to the overall bond valence[49,50] of them. A nice example is Te12 in $Ce_2Te_3O_9$,

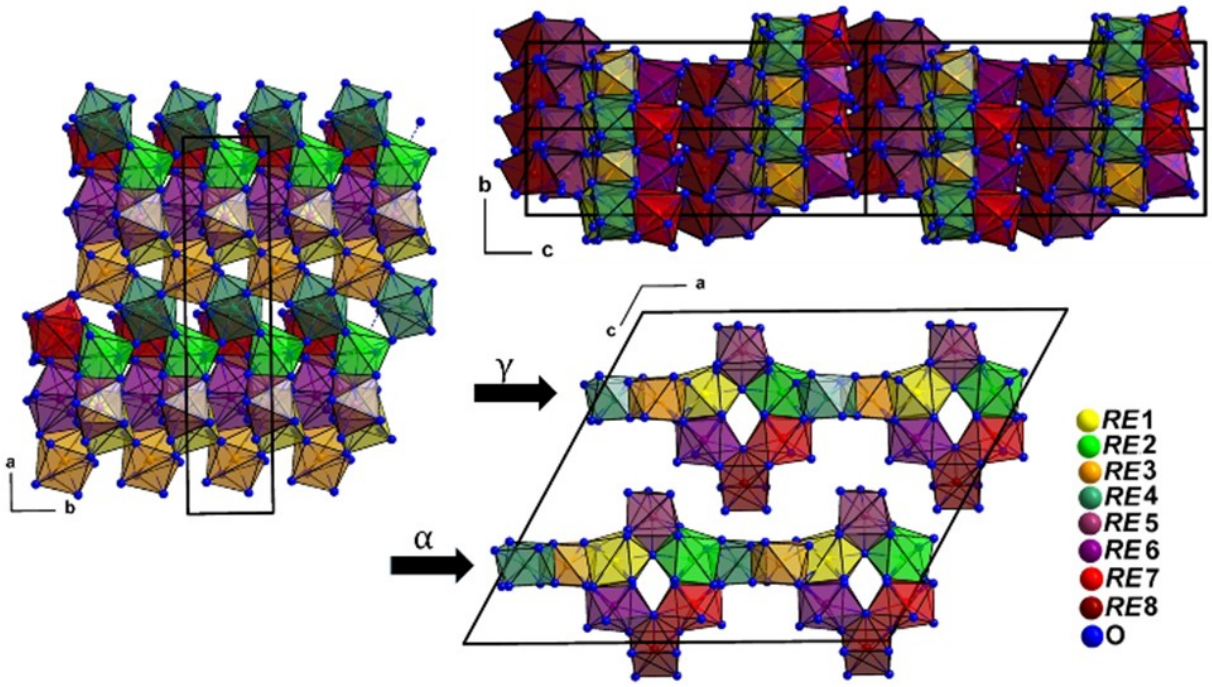

Figure 7. Five chains ($4\times{}^{1}_{\infty}\{[RE_2O_{13}]^{20-}\}$ and $1\times{}^{1}_{\infty}\{[RE_2O_{12}]^{18-}\}$) forming corrugated ${}^{2}_{\infty}\{[RE_8O_{35}]^{46-}\}$ layers parallel to (001) plane in the A2-type crystal structure (*left*) for the composition $RE_2Te_3O_9$ (RE = Pr and Nd). The graph shows the corrugated ${}^{2}_{\infty}\{[RE_8O_{35}]^{46-}\}$ sheets in top view at α- and γ-layers parallel to the (010) plane (*bottom right*) and the side view of the *c*-glide plane, which runs parallel to the [001] direction (*top right*).

for which the bond-valence sum with just O34, O35 and O36 in its discrete $[(Te12)O_3]^{2-}$ anion amounts to only 3.62 valence units. Keeping in mind that valence sums by 10 % away from their ideal values indicate missing bonds, the inclusion of four more bonds to the oxygen atoms O11, O22, O23 and O25, more or less all on the lone-pair side and at distances of $d \geq 300$ pm from $(Te12)^{4+}$, raises the bond-valence sum to 3.85 valence units, being a lot closer to the ideal value of 4.

Conclusions

In summary, our work describes the solid-state synthesis and crystal structures of two new structure types for the composition $RE_2Te_3O_9$: A1-type (RE = La and Ce) versus A2-type (RE = Pr and Nd). Despite the fact that both structure types contain similar fundamental building blocks (FBBs) of rare-earth metal-oxygen polyhedra and ψ^1-tetrahedral oxotellurate(IV) units with secondary bonding interactions (SBIs), which also lead to similar ${}^{2}_{\infty}\{[RE_8O_{35}]^{46-}\}$ layers and one-dimensional oxotellurate(IV) partial structures, the arrangements of both within the structures are slightly different. This is due to the different space groups $P2_1$ for the A1-type and *Cc* for the A2-type structure, which result from different symmetry operations such as a 2_1 screw axis and a *c*-glide plane, respectively. Besides this, the presence of strong secondary $Te^{4+}\cdots O^{2-}$ interactions in these rare-earth metal(III) oxotellurates(IV) strengthen the stability of their crystal structures, which make them good candidates as host materials for luminescence applications. In our future work, we will try to synthesize phase-pure $La_2Te_3O_9$ and dope it with Ce^{3+} or Pr^{3+} cations to see their suitability in use as scintillators or luminescing materials. Since both Ce^{3+} and Pr^{3+} cations have a similar size to La^{3+} cations, they should be able to substitute them very well. Less matching cations like Eu^{3+} or Tb^{3+} could cause a visible red or green luminescence, when incorporated into the $La_2Te_3O_9$ host lattice. The major advantage of using oxotellurates(IV) as host material is the fact, that the doped cation has not to be excited directly (usually in a very small energetic range), but the excitation can also take place in the region of the broad O–Te charge-transfer band and/or on the lone-pair electrons at the Te^{4+} cations, providing the so-called "inorganic antenna effect".[55] Therefore an enhanced luminescent efficacy is expected to be observed, just like in the case of the rare-earth metal(III) oxoantimonate(III) bromides $RESb_2O_4Br$ (RE = Eu–Tb),[56] where Sb^{3+} plays a similar role as its isoelectronic Te^{4+} neighbour in the periodic system of the elements (PSE).

We did not comment much on the function of the lone pairs in these A-type crystal structures for the composition $RE_2Te_3O_9$ (RE = La–Nd), but this will be discussed in a consecutive article dealing with the B-type and C-type structures for the heavier $RE_2Te_3O_9$ representatives (B-type: RE = Sm–Er and Y, C-type: RE = Tm–Lu, D-type: RE = Sc)[57] for comparison. Having dedicated the present publication to *Sven Lidin* on the occasion of his 60th anniversary, we need to find some proper words, however, best by quoting the birthday boy himself. "Com-

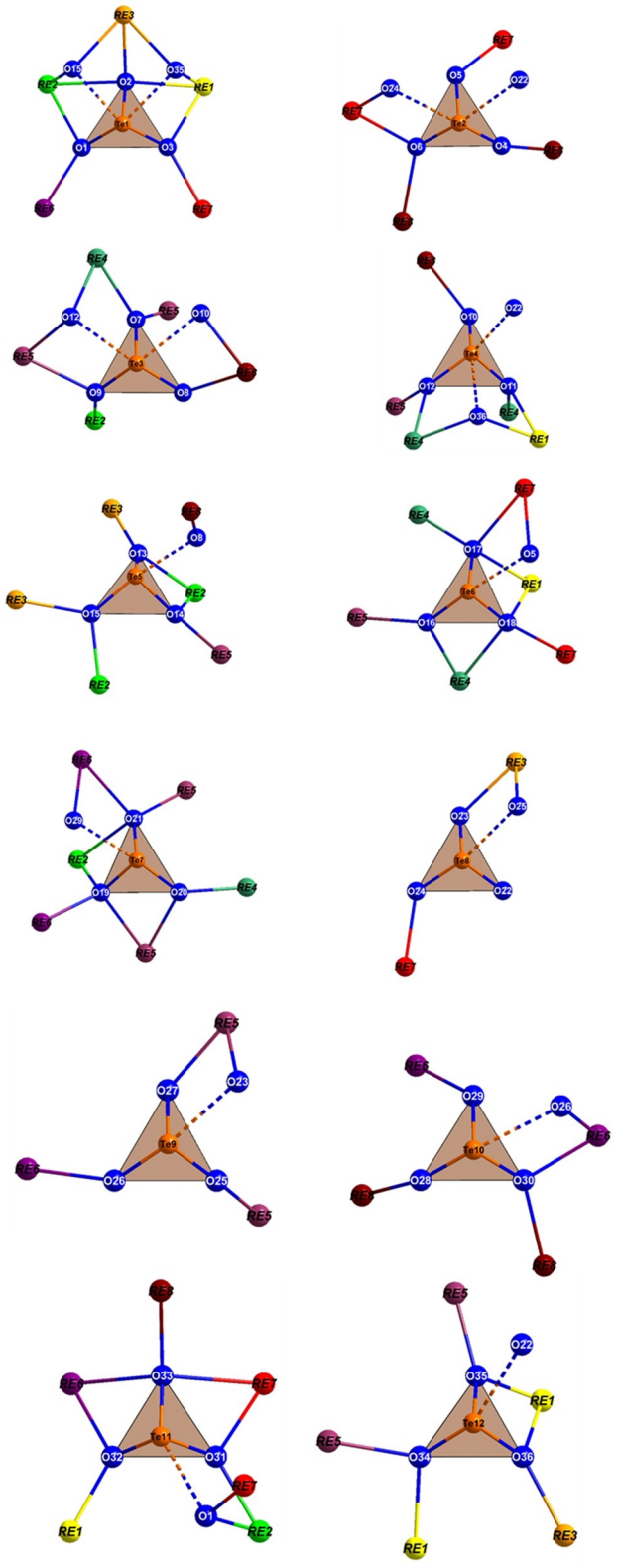

Figure 8. Coordination polyhedra of the twelve crystallographically different Te^{4+} cations in A2-type crystal structure for the composition $RE_2Te_3O_9$ (RE = Pr and Nd), where twelve $[TeO_3]^{2-}$ units are linked through strong secondary $Te^{4+}\cdots O^{2-}$ contacts (*dashed bonds*), with their complete cationic surrounding.

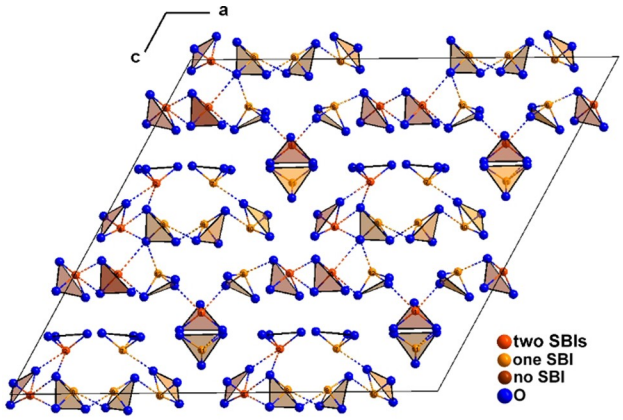

Figure 9. Through strong secondary $Te^{4+}\cdots O^{2-}$ contacts $^1_\infty\{[Te_{12}O_{36}]^{24-}\}$ strands are formed propagating along [010] direction in the A2-type crystal for the composition $RE_2Te_3O_9$ (RE = Pr and Nd) structure involving all twelve $[TeO_3]^{2-}$ units.

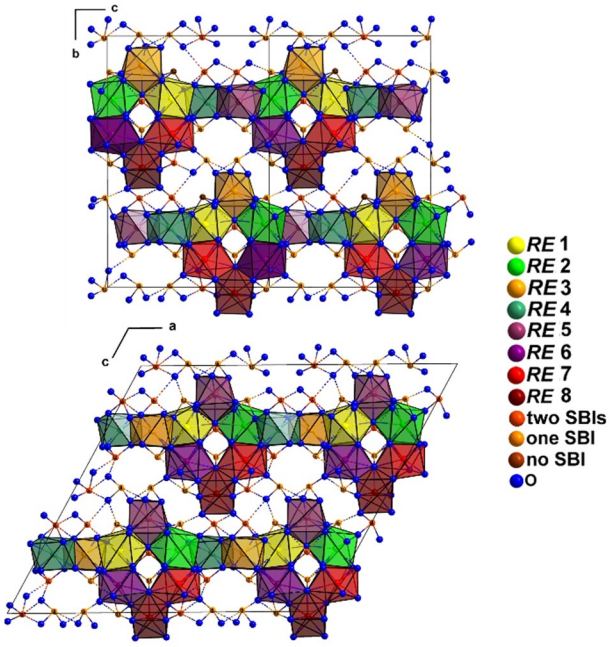

Figure 10. The surface network $^2_\infty\{[RE_2O_9]^{12-}\}$ of the A1-type crystal structure for the composition $RE_2Te_3O_9$ (RE = La and Ce) (*top)* and the A2-type crystal structure for the composition $RE_2Te_3O_9$. (RE = Pr and Nd) (*bottom*). For the charge balance, twelve Te^{4+} cations are to be taken into account per formula unit.

pounds containing main-group metals in low oxidation states frequently exhibit stereochemically active lone pairs. In particular, this is observed for compounds of Sn^{II}, Pb^{II}, As^{III}, Sb^{III}, Bi^{III}, and Te^{IV}. An intriguing phenomenon is the localization of such lone pairs to well defined regions of the solid-state structures of these compounds, wherein the volumes of lone pairs form surfaces that separate regions of different kinds of chemical interaction. Interestingly, lone pairs tend to aggregate and even more so, they tend to aggregate together with negatively

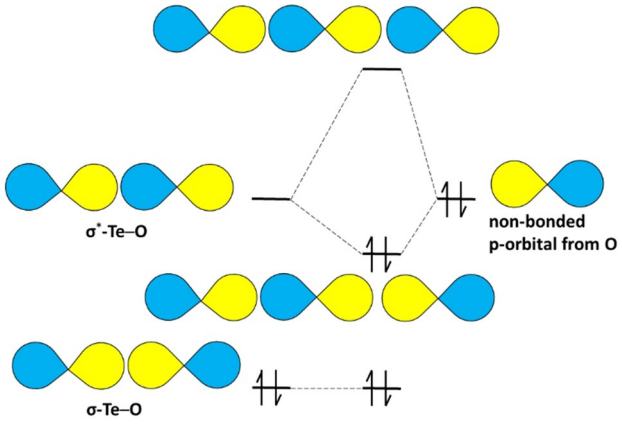

Figure 11. The secondary bonding interaction (SBI) originates from the hyperconjugation of a σ*-Te–O molecular orbital with a non-bonded p-orbital from an oxygen atom (according to [45]). The colors for the orbitals are referring to the Swedish flag of *Sven Lidin*'s home country.

charged ions."[58] In other words: "lone pairs tend to flock together, because nobody else likes them". With this jolly verbal phrase from *Sven Lidin* at some inorganic solid-state conference, we want to encourage him to find these very compartments in our A-type crystal structures for the composition $RE_2Te_3O_9$ on his own.

Experimental Section

Synthesis

The new rare-earth metal(III) oxotellurates(IV) $RE_2Te_3O_9$ (RE = La–Nd) were obtained through solid-state reactions from the mixtures of the corresponding binary oxides with cesium chloride as fluxing agent. Their reaction equations can be described as follows:

$$RE_2O_3 + 3\ TeO_2 \rightarrow RE_2Te_3O_9\ (RE = \text{La and Nd}) \quad (1)$$

$$3\ CeO_2 + Ce + 6\ TeO_2 \rightarrow 2\ Ce_2Te_3O_9 \quad (2)$$

$$3\ Pr_6O_{11} + 4\ Pr + 33\ TeO_2 \rightarrow 11\ Pr_2Te_3O_9 \quad (3)$$

All the chemicals are commercially available, which includes La_2O_3 (ChemPur: 99.999%), Nd_2O_3 (Heraeus: 99.9%), CeO_2 (ChemPur: 99.9%), Pr_6O_{11} (ChemPur: 99.9%), Ce (ChemPur: 99.9%), Pr (ChemPur: 99.9%), TeO_2 (Alfa Aesar: 99.99%) and CsCl (Merck: 99.99%). The reaction mixtures were prepared and filled into fused silica ampoules under the inert argon atmosphere of a glove box (M. Braun). The silica ampoules were torch-sealed under dynamic vacuum and heated up to 850 °C in 8 hours. The annealing duration lasted for 10 days. After slowly cooling down with 5 °C/h to 450 °C and then quickly to room temperature, needle-shaped single crystals (Figure 1) of the $RE_2Te_3O_9$ representatives (RE = La: colorless, Ce: pale yellow, Pr: pale green, Nd: pale violet) were obtained, which remained stable in air and water. Thus the CsCl flux could be easily washed out by rinsing the crude products with demineralized water.

Crystal-Structure Analysis

A STADI P powder X-ray diffractometer from Stoe equipped with germanium-monochromatized Cu-K_α radiation (wavelength: λ = 154.06 pm) and a position-sensitive detector were used for the purity check of the samples. However, all attempts to prepare single-phase samples of the title compounds remained unsatisfying, so far. According to powder X-ray diffraction (PXRD) the thermodynamically more stable phases $RE_2Te_4O_{11}$[22] (RE = La–Nd) could always be detected in the final products with a share of almost 10%. Figure 12 shows a PXRD of the water-rinsed product of A1-type $La_2Te_3O_9$, which consists to 90% of the target compound and to 10% of $La_2Te_4O_{11}$.[22] In exchange, TeO_2-poorer phases like $La_{10}Te_{12}O_{39}$[59] or $La_2Te_2O_7$[31] can be found as low-quality single crystals.

Intensity data sets for single crystals of the title compounds were collected with a Nonius Kappa-CCD X-ray diffractometer using graphite-monochromatized Mo-K_α radiation (wavelength: λ = 71.07 pm). A numerical absorption correction was performed with the program HABITUS[51] in all four cases. Structure solutions and refinements were carried out by using the program package SHELX-97.[52,60] Details of the data collections and the structure refinements[53] of the $RE_2Te_3O_9$ representatives with RE = La–Nd are summarized in Tables 1–6. All heavy atoms (RE and Te) could be refined smoothly with anisotropic displacement parameters (U_{ij}), while for the oxygen atoms, always just isotropic ones (U_{iso}) have been applied, avoiding to overstress the ratio of refined parameters N to unique reflections (see Tables 1 and 2 for the individual $RE_2Te_3O_9$ representatives) from N = 505–507 to N = 325–327. Owing to the non-centrosymmetry of both space groups ($P2_1$ and Cc), twin refinements[52] were necessary to improve the structure convergence in most cases. So for $La_2Te_3O_9$ the twin matrix (100 0$\bar{1}$0 $\bar{1}$0$\bar{1}$) was applied, while the crystals of $Pr_2Te_3O_9$ and $Nd_2Te_3O_9$ have been treated as inversion twins (matrix: $\bar{1}$00 0$\bar{1}$0 00$\bar{1}$). Only the $Ce_2Te_3O_9$ crystal with a *Flack x* parameter of about −0.03 (Tables 1 and 2) was considered to occur untwinned. A certain incompleteness of X-ray diffraction data for A1-type $Ce_2Te_3O_9$ results from the fact that we here tried to collect high diffraction-angle reflections with $2\theta_{max} \approx 65.5°$ (as compared to $2\theta_{max} \approx 56.6°$ for $La_2Te_3O_9$, Tables 1 and 2)

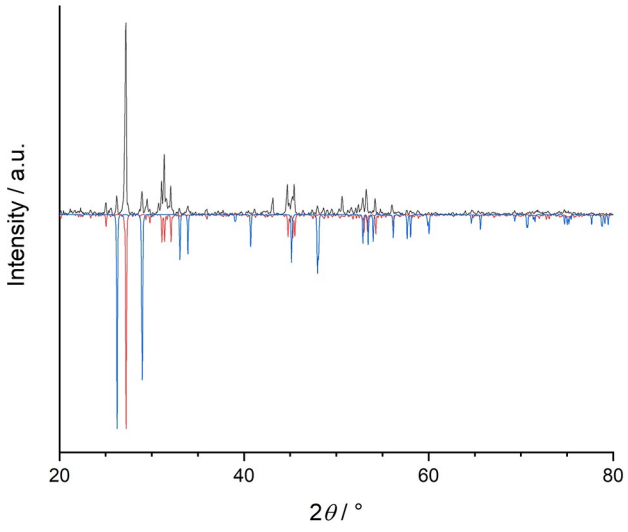

Figure 12. Powder X-ray diffractogram (PXRD) of a $La_2Te_3O_9$ sample (positive peaks, black). The negative peaks were calculated with the data from Tables 1–6 for $La_2Te_3O_9$ (red) and from *Meier et al.* [22] for $La_2Te_4O_{11}$ (blue).

in order to exploit anomalous dispersion for establishing the non-centrosymmetric space group $P2_1$ with a maximum of *Miller* indices of $\pm h = 7$, $\pm k = 33$, $\pm l = 22$ for $Ce_2Te_3O_9$ versus $\pm h = 7$, $\pm k = 29$, $\pm l = 19$ for $La_2Te_3O_9$. With the short *a*-axis oriented as long-needle direction on the diffractometer, there were not enough reflections with higher $\pm h$ numbers to secure a sufficient data completeness. So with only 26006 measured reflections for $Ce_2Te_3O_9$ versus 29098 ones for $La_2Te_3O_9$ we gained 10880 unique ones for $Ce_2Te_3O_9$ versus 8527 unique ones for $La_2Te_3O_9$ (Tables 1 and 2). As a result we reached a nice *Flack x* parameter of −0.0261(5) for $Ce_2Te_3O_9$ versus 0.1605(6) for $La_2Te_3O_9$ (Tables 1 and 2), but a data completeness of only 92.4 % for $Ce_2Te_3O_9$ versus almost 100 % for $La_2Te_3O_9$.

Fractional atomic coordinates, coefficients of the displacement parameters, selected interatomic distances and important bond angles for A1-type $La_2Te_3O_9$ and $Ce_2Te_3O_9$ as well as A2-type $Pr_2Te_3O_9$ and $Nd_2Te_3O_9$ are given in the Tables 7–14, respectively. More details of the crystal-structure investigations for all four of the A-type $RE_2Te_3O_9$ members (*RE* = La–Nd) can be obtained from the Fachinformationszentrum (FIZ) Karlsruhe, D-76344 Eggenstein-Leopoldshafen, Germany (E-Mail: crysdata@fiz-karlsruhe.de), under the CSD numbers given in the Tables 1–6.

Single-Crystal Raman Spectroscopy

A colorless single crystal of $La_2Te_3O_9$ was taken to record a single-crystal Raman spectrum on a XploRA device from Horiba Jobin Yvon (Figure 13). The used wavelength originated from a red LASER (Light Amplification by Stimulated Emission of Radiation) with $\lambda =$ 638 nm.

If one ignores all secondary bond interactions between Te^{4+} and O^{2-} with *d*(Te–O) > 195 pm (see Tables 7–10) $La_2Te_3O_9$ could well be written as $La_2[TeO_3]_3$, but at the latest, its single-crystal Raman spectrum (Figure 13) tells you a different story. As compared with the free $[TeO_3]^{2-}$ anion in aqueous solution exhibiting C_{3v} symmetry ($\nu_s \approx 758$ cm^{-1}, $\nu_{as} \approx 703$ cm^{-1}, $\delta_s \approx 364$ cm^{-1} and $\delta_{as} \approx 326$ cm^{-1})[61,62] or the discrete one in solid $Na_2[TeO_3]$ (monoclinic, $P2_1/c$; *d*(Te–O) = 187–189 pm, ∢(O–Te–O) = 96–99°, *d*(Te–(O,O,O)) = 92.5 pm, *d*(Te···O) = 291–310 pm),[63] a lot more vibrational bands can be detected.

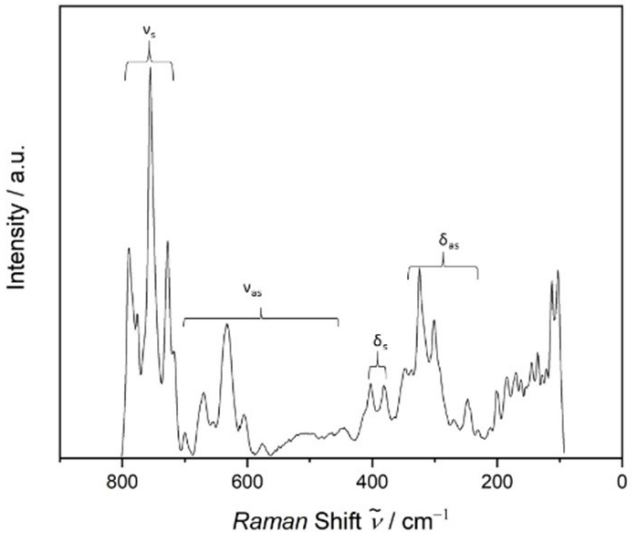

Figure 13. Single-crystal Raman spectrum of $La_2Te_3O_9$.

The free $[TeO_3]^{2-}$ anion with C_{3v} point symmetry has irreducible representations (irreps) for the vibrational degrees of freedom like

$$\Gamma_{vib} = 2\ A_1 \ \oplus\ 2\ E.$$

Thus both of the irreps (A_1 and E) are IR- and Raman-active. The irrep A_1 is totally symmetric, since all characters for all symmetry operations are +1 in the character table. A_1 represents a one-dimensional character, whereas *E* stands for a two-dimensional one. The index 1 indicates a C_2-axis or a vertical mirror plane σ_v, which stands perpendicular to the principle axis. After the symmetry operations an unchanged sign in the *Cartesian* coordinate system emerges. Since in the A1-type crystal structure of $La_2Te_3O_9$ a symmetry reduction is observed to the point symmetry C_1 or C_s, four broader ranges are expected. Both of the irreps A_1 represent a symmetric stretching vibration ν_s and a symmetric bending vibration δ_s. Both of the irreps *E* depict degenerate state for the asymmetric stretching vibration ν_{as} and the asymmetric deformation vibration δ_{as}. Thus a split of the degenerate modes has to be expected. So according to this, we find the respective Raman shifts in the following ranges: $\nu_S \approx 791$–728 cm^{-1}, $\nu_{as} \approx 699$–443 cm^{-1}, $\delta_S \approx 403$–380 cm^{-1} and $\delta_{as} \approx 349$–228 cm^{-1} (see Figure 13). Raman shifts at lower wavenumbers result from lattice vibrations based on La^{3+}–O^{2-} bonds.

Acknowledgements

We thank Dr. Falk Lissner (AOR) for the single-crystal X-ray diffraction measurements, Felix C. Goerigk (M. Sc) for his scanning electron microscopy (SEM), Kevin U. Bareiß (M. Sc.) for recording the single-crystal Raman spectra, Dr. Sabine Zitzer, now Metzger (Ledvance GmbH, Garching, Germany), for her helpful advice concerning the crystallization experiments, and the State of Baden-Württemberg (Stuttgart, Germany) for its financial support. Open access funding enabled and organized by Projekt DEAL.

Keywords: Lanthanum · Cerium · Praseodymium · Neodymium · Oxotellurates(IV) · Crystal structure · Stereochemical lone-pair activity

[1] G. B. Nikiforov, A. M. Kusainova, P. S. Berdonosov, V. A. Dolgikh, P. Lightfoot, *J. Solid State Chem.* **1999**, *146*, 473–477.
[2] O. Lindqvist, *Acta Chem. Scand.* **1968**, *22*, 977–982.
[3] H. Beyer, *Z. Kristallogr.* **1967**, *124*, 228–237.
[4] T. G. Worlton, R. A. Beyerlein, *Phys. Rev.* **1975**, *B 12*, 1899–1907.
[5] K. Hanke, *Naturwissenschaften* **1967**, *54*, 199.
[6] E. M. Walitzi, *Tschermaks Mineral. Petrogr. Mitt.* **1965**, *10*, 241–255.
[7] J. Zemann, *Monatsh. Chem.* **1971**, *102*, 1209–1216.
[8] V. A. Dolgikh, *Russ. J. Inorg. Chem.* **1991**, *36*, 1117–1123.
[9] A. V. Marukhnov, D. V. Pushkin, V. N. Serezhkin, *Russ. J. Inorg. Chem.* **2007**, *52*, 203–208.
[10] M. S. Wickleder, *Chem. Rev.* **2002**, *102*, 2011–2087.
[11] M. S. Wickleder, O. Büchner, C. Wickleder, S. el Sheik, G. Brunklaus, H. Eckert, *Inorg. Chem.* **2004**, *43*, 5860–5864.
[12] P. M. Almond, M. L. McKee, T. E. Albrecht-Schmitt, *Angew. Chem. Int. Ed.* **2002**, *41*, 3426–3429; *Angew. Chem.* **2002**, *114*, 3576–3579.

[13] Y. Porter, K. M. Ok, N. S. P. Bhuvanesh, P. S. Halasyamani, *Chem. Mater.* **2001**, *13*, 1910–1915.
[14] K. M. Ok, P. S. Halasyamani, *Chem. Mater.* **2002**, *14*, 2360–2364.
[15] E. O. Chi, K. M. Ok, Y. Porter, P. S. Halasyamani, *Chem. Mater.* **2006**, *18*, 2070–2074.
[16] W. T. A. Harrison, L. L. Dussack, A. J. Jacobson, *J. Solid State Chem.* **1996**, *125*, 234–242.
[17] V. Balraj, K. Vidyasagar, *Inorg. Chem.* **1999**, *38*, 5809–5813.
[18] P. Höss, A. Osvet, F. Meister, M. Batentschuk, A. Winnacker, Th. Schleid, *J. Solid State Chem.* **2008**, *181*, 2783–2788.
[19] S. Zitzer, *Doctoral Dissertation*, Univ. Stuttgart, Stuttgart **2011**.
[20] A. Castro, R. Enjalbert, D. Lloyd, I. Rasines, J. Galy, *J. Solid State Chem.* **1990**, *85*, 100–107.
[21] I. Ijjaali, C. Flaschenriem, J. A. Ibers, *J. Alloys Compd.* **2003**, *354*, 115–119.
[22] S. F. Meier, Th. Schleid, *Z. Naturforsch.* **2004**, *59b*, 881–888.
[23] P. Höss, S. F. Meier, Th. Schleid, *Z. Kristallogr.* **2004**, *S 21*, 162–162.
[24] Y. L. Shen, J. G. Mao, *J. Alloys Compd.* **2004**, *385*, 86–89.
[25] P. Höss, G. Starkulla, Th. Schleid, *Acta Crystallogr.* **2005**, *E 61*, i113–i114.
[26] F. A. Weber, Th. Schleid, *Z. Kristallogr.* **2000**, *S 17*, 136–136.
[27] F. A. Weber, S. F. Meier, Th. Schleid, *Z. Anorg. Allg. Chem.* **2001**, *627*, 2225–2231.
[28] S. F. Meier, Th. Schleid, *Z. Naturforsch.* **2005**, *60b*, 720–726.
[29] P. Höss, S. F. Meier, Th. Schleid, *Z. Kristallogr.* **2005**, *S 22*, 153–153.
[30] P. Höss, Th. Schleid, *Z. Anorg. Allg. Chem.* **2007**, *633*, 1391–1396.
[31] F. A. Weber, Th. Schleid, *Z. Anorg. Allg. Chem.* **2000**, *626*, 1285–1287.
[32] M. J. Redman, W. P. Binnie, J. R. Carter, *J. Less-Common Met.* **1968**, *16*, 407–413.
[33] P. Höss, *Doctoral Dissertation*, Univ. Stuttgart, Stuttgart **2010**.
[34] S.-C. Chou, *Doctoral Dissertation*, Univ. Stuttgart, Stuttgart **2016**.
[35] S. F. Meier, *Doctoral Dissertation*, Univ. Stuttgart, Stuttgart **2002**.
[36] S. F. Meier, P. Höss, Th. Schleid, *Z. Anorg. Allg. Chem.* **2009**, *635*, 768–775.
[37] P. Höss, Th. Schleid, *Z. Anorg. Allg. Chem.* **2008**, *634*, 2047–2047.
[38] P. Höss, S. F. Meier, Th. Schleid, *Z. Anorg. Allg. Chem.* **2013**, *639*, 2548–2553.
[39] S. Y. Song, D. W. Lee, K. M. Ok, *Inorg. Chem.* **2014**, *53*, 7040–7046.
[40] S.-C. Chou, Th. Schleid, *Z. Kristallogr.* **2014**, *S 34*, 131–131.
[41] N. W. Alcock, *Adv. Inorg. Chem.* **1972**, *15*, 1–58.
[42] A. G. Christy, S. J. Mills, A. R. Kampf, *Mineral. Mag.* **2016**, *80*, 415–545.
[43] I. D. Brown, *J. Solid State Chem.* **1974**, *11*, 214–233.
[44] J. Zuckerman, I. Haiduc, *Phosphorus Sulfur Silicon Relat. Elem.* **2001**, *171*, 73–112.
[45] A. F. Cozzolino, P. J. W. Elder, I. Vargas-Basca, *Coord. Chem. Rev.* **2011**, *225*, 1426–1438.
[46] L. Vogel, P. Wonner, S. M. Huber, *Angew. Chem.* **2019**, *58*, 1880–1891.
[47] M. K. Si, B. Ganguly, *New J. Chem.* **2016**, *40*, 9132–9138.
[48] J. Bamberger, F. Ostler, O. G. Mancheño, *ChemCatChem* **2019**, *11*, 5198–5211.
[49] I. D. Brown, D. Altermatt, *Acta Crystallogr.* **1991**, *B 41*, 244–247.
[50] N. E. Brese, M. O'Keeffe, *Acta Crystallogr.* **1991**, *B 47*, 192–197.
[51] W. Herrendorf, H. Bärnighausen, HABITUS: Program for the Optimization of the Crystal Shape for Numerical Absorption Correction in X-SHAPE, Version 1.06, Stoe, Darmstadt **1999**, Karlsruhe **1993**, Gießen **1996**.
[52] G. M. Sheldrick, SHELXS-97 and SHELXL-97: Programs for Solution and Refinement of Crystal Structures from X-Ray Diffraction Data, Göttingen **1997**.
[53] *International Tables for Crystallography*, *Vol. C* (Eds.: T. Hahn, A. J. C. Wilson), 2nd Ed., Kluwer Academic Publishers, Dordrecht, Boston, London **1992**.
[54] R. Herbst-Irmer, G. M. Sheldrick, *Acta Crystallogr.* **1998**, *B 54*, 443–449.
[55] I. Hartenbach, S. Strobel, Th. Schleid, B. Sarkar, W. Kaim, P. Nockemann, K. Binnemans, P. K. Dorhout, *Eur. J. Inorg. Chem.* **2010**, *2010*, 1626–1632.
[56] F. C. Goerigk, V. Paterlini, K. V. Dorn, A.-V. Mudring, Th. Schleid, *Crystals* **2020**, *10*, 1089–1111.
[57] S.-C. Chou, P. L. Russ, Th. Schleid, *Z. Naturforsch.* **2021**, *76b*, in preparation.
[58] Z. Mayerová, M. Johnsson, S. Lidin, *Angew. Chem. Int. Ed.* **2006**, *45*, 5602–5606; *Angew. Chem.* **2006**, *118*, 5730–5734.
[59] P. L. Wang, Y. Mozharivskyj, *Acta Crystallogr.* **2013**, *E 69*, i36.
[60] G. M. Sheldrick, *Acta Crystallogr.* **2008**, *A 64*, 112–122.
[61] J. Weidlein, U. Müller, K. Dehnicke, *Schwingungsfrequenzen I*, 1. Auflage, Georg-Thieme-Verlag, Stuttgart, New York **1981**.
[62] H. Siebert, *Anwendung der Schwingungsspektroskopie in der Anorganischen Chemie*, Springer-Verlag, Berlin, Heidelberg, New York **1996**.
[63] R. Masse, J. C. Guitel, I. Tordjman, *Mater. Res. Bull.* **1980**, *15*, 431–436.

Manuscript received: October 20, 2020
Revised manuscript received: January 19, 2021

